One–Dimensional Nonlinear Finite Strain Analysis of Self–Weight Consolidation of Soft Clay Considering Creep

Penglin LI, PhD candidate

Department of Civil and Environmental Engineering, The Hong Kong Polytechnic University, Hung Hom, Kowloon, Hong Kong, China; email: 21036922R@connect.polyu.hk

Jian-Hua Yin, Chair Professor

Department of Civil and Environmental Engineering, The Hong Kong Polytechnic University, Hung Hom, Kowloon, Hong Kong, China; email: jian-hua.yin@polyu.edu.hk

Zhen-Yu Yin, Professor

Department of Civil and Environmental Engineering, The Hong Kong Polytechnic University, Hung Hom, Kowloon, Hong Kong, China; email: zhenyu.yin@polyu.edu.hk

Corresponding author, Tel: +852 3400 8470; Fax: +852 2334 6389

Zejian Chen, PhD candidate

Department of Civil and Environmental Engineering, The Hong Kong Polytechnic University, Hung Hom, Kowloon, Hong Kong, China; email: ze-jian.chen@connect.polyu.hk

Revised manuscript submitted to *Computers and Geotechnics*

21 May 2022

Abstract:

Creep as an intrinsic property of clay is non–negligible in predicting ground settlements in land reclamation construction and foundations on reclaimed land and soft soils, but it is unfortunately difficult to characterize in current self–weight consolidation analysis. This paper develops a one–dimensional (1D) finite strain consolidation model to take into account the creep of soft clay, particularly during the early stages of reclamation construction, mainly in a self-weight consolidation process. In this model, the Yin–Graham 1D Elastic Visco-Plastic (EVP) model is first extended for modelling self-weight finite strain consolidation of soft clays to describe the creep of soil skeleton under extremely high water content. The Darcian and non-Darcian flow, nonlinear compressibility and permeability of soft clays with a huge variety of water content are also considered. Governing partial differential equations using the EVP model are derived. These nonlinear partial differential equations are solved using the Crank–Nicholson finite difference method. Three case studies involving a wide range of initial void ratio values are simulated, which show that the present model, with more realistic consideration of creep feature of clays than previous ones, can capture the self-weight consolidation process well when compared with physical model test results. The influences of the initial height and void ratio on the self-weight consolidation process are analyzed to provide some recommendations for engineering practice.

Keywords: finite strain; creep; soft clay; self–weight consolidation; viscoplasticity; permeability

Introduction

To compensate for the short supply of sand in coastal cities, local marine deposits are widely used to fill portions of reclaimed areas using the dredging and pumping method. During the reclamation, the local marine deposits that are in a slurry state usually undergo settling, self–weight consolidation, and accelerated consolidation with vertical drains and pre–loading. One–dimensional (1D) self–weight consolidation is highly significant during the early stages of reclamation that use marine deposits as fill material. Vrakas and Anagnostou (2015) pointed that the small strain theory is not suitable once the strain exceeds 10%. In addition, the finite strain theory is more appropriate when the soil has a large initial water content higher than liquid limit generally resulting in large settlement. During the self–weight consolidation process, dredged soft soil settles significantly relative to the thickness of the soil layer. Moreover, in cases featuring obvious changes in void ratio, compressibility and permeability can be found to have a nonlinear relationship with the void ratio. Accordingly, the self–weight consolidation of slurry is a finite strain problem instead of a small strain problem. Furthermore, soft soil exhibits evident creep that inevitably causes inaccurate assessment of settlement and stress distribution if not taken into account (Bjerrum, 1967, 1973) in the consolidation theory. The creep of soil is mainly due to interparticle sliding, the expulsion of water from double layers of clay particles, and the rearrangement of adsorbed water molecules and cations into different positions that are time-dependent. Sills (1995) presented several experimental investigations that the settlement induced by creep was comparable with that due to the effective stress, and creep settlement is theoretically important in cases of self–weight

consolidation since creep is an intrinsic property of clay. Therefore, an accurate prediction for self–weight consolidation process considering creep of soft clay is needed for engineering design, construction control and safety assessment of structures on or in reclaimed land.

Developing a consolidation prediction method has historically been highly challenging. Terzaghi (1943) proposed a 1D consolidation theory based on a series of simplifying assumptions, including small strain assumption, which are approximately applicable in practice. Richard (1957) and McNabb (1960) were among the first to consider finite strain consolidation problems in soil, although the details of 1D finite strain consolidation governing equations that treat void ratio as the main variable were proposed and obtained by Gibson et al. (1967, 1981). Many governing equations for 1D primary consolidation of saturated thick soil layers that have been advocated from time to time are either equivalent to or special cases of the finite strain consolidation governing equations proposed by Gibson et al. (1967, 1981) (e.g., Schiffman, 1980; Cargill, 1986; McVay et al., 1986). However, the soil skeleton in the foregoing consolidation analysis were considered elastic.

Carter et al. (1979) presented a numerical method for analysing finite elasto–plastic consolidation, and Borja et al. (1994), Borja and Alarcon (1995) and Borja et al. (1998) successfully developed a mathematical framework and finite element method for finite strain consolidation analysis using an elasto–plastic model with some case studies. Fox and colleagues (Fox and Berles, 1997; Fox, 1999; Fox et al., 2014) and Pu et al. (2020) developed dimensionless piecewise–linear numerical models, named CS2 and CS3, for 1D finite strain consolidation analysis. Both CS2 and CS3 accounted for large strain, self–weight of soil, elastic

or elasto–plastic constitutive modelling, the relative velocities of the fluid and solid phases and variable hydraulic conductivity and compressibility during the consolidation process. Although Hawlader et al. (2003) developed a 1D consolidation model considering viscosity effects of clay based on a strain rate dependent constitutive model. However, from then few works investigated or even considered the time–dependent nonlinear creep of clayey soils (an intrinsic property of clay) in the context of self–weight finite strain consolidation problems starting from a high initial water content.

In this paper, a 1D finite strain consolidation theory is developed and verified that takes into account creep for self–weight consolidation of soft clay. Firstly, the 1D Yin–Graham EVP model is extended for the finite strain case by modifications of two logarithmic functions of instant and reference time lines for the creep equation. Secondly, the existing 1D finite strain consolidation theory is extended to consider creep, self–weight, changing compressibility and hydraulic conductivity of slurry by incorporating the extended 1D EVP model. Nonlinear partial differential equations are then solved using the Crank–Nicholson finite difference method. The extended 1D finite strain consolidation model is applied to simulate three case studies. Further, some parametric studies of the proposed consolidation model are conducted.

1D finite strain consolidation theory accounting for creep

Coordinate systems

Figure 1 shows a saturated soil layer in Lagrangian coordinates and convective coordinates: (a) initial configuration at $t = 0$ with vertical Lagrangian coordinate a, $a = 0$ at the

soil surface and $a = a_0$ at the soil bottom; (b) configuration at time t with vertical convective coordinate ξ.

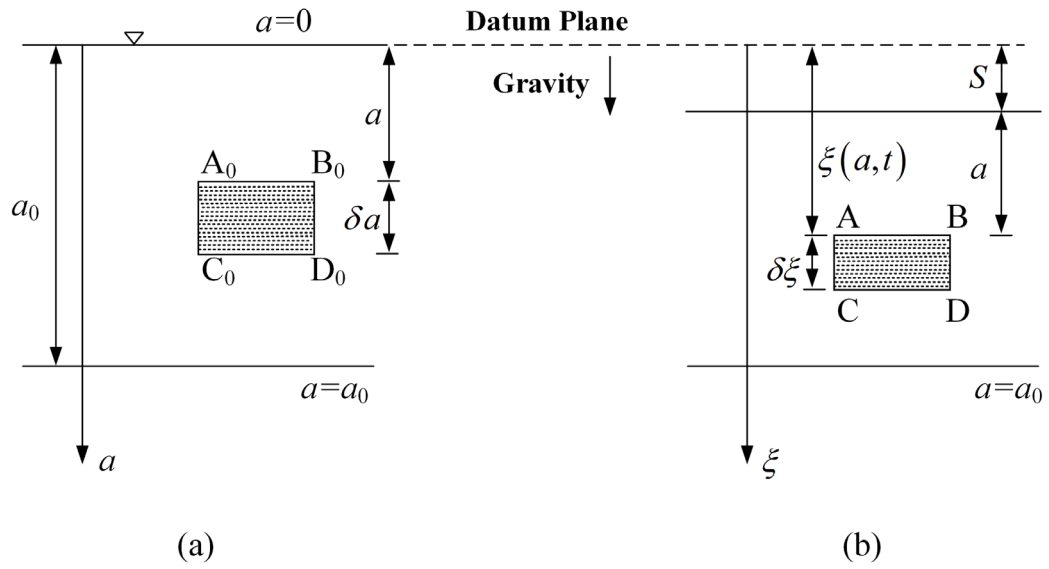

Figure 1–Lagrangian coordinates for finite strain consolidation theory: (a) initial configuration at $t = 0$ and (b) configuration at time t (also called convective coordinate)

The coordinate system generally used in geotechnical engineering is the Eulerian system, in which material deformation is related to planes fixed in space. A real measuring system is one that connects with the material particles, especially under finite strain. Small strain consolidation theory assumes that a clay layer's deformation is small compared with its thickness, removing the need to distinguish among Eulerian systems, Lagrangian systems and convective coordinates. For finite strain problems in geotechnical engineering, however, changes in surface height are large compared with the thickness of the soil layer, so that the Eulerian system is no longer applicable. Furthermore, there are also several obvious advantages of using Lagrangian coordinates instead of convective coordinates. Firstly, there is no need to

consider the coordinate change of the soil surface with the consolidation process in Lagrangian coordinates, because the soil surface is always at $a = 0$.

Secondly, Lagrangian coordinate a is an independent variable, whereas convective coordinate ξ is dependent on a and t: $\xi = \xi(a, t)$. These advantages of the Lagrangian coordinate system will aid mathematical analysis of finite strain consolidation. Converting variables expressed in Lagrangian coordinates into the convective system is straightforward using the relationship between a and ξ given by Gibson et al. (1967, 1981),

$$\frac{\partial \xi}{\partial a} = \frac{1+e}{1+e_0} \tag{1}$$

where e is the void ratio of the clay layer at (a, t) and e_0 the initial void ratio of the clay layer.

It is also evident that convective coordinate ξ and Lagrangian coordinate a are related to the settlement S of the soil layer from Figure 1:

$$\xi = a + S \tag{2}$$

1D finite strain consolidation theory

Firstly, we introduce some general equations in convective coordinates. Considering a current infinitesimal element of ABCD at t in Figure 1(b), changed from the initial element $A_0B_0C_0D_0$ at $t = 0$ in Figure 1(a) and the vertical force equilibrium of a soil particle, we obtain (Gibson et al., 1967; Yin and Zhu, 2020)

$$\frac{\partial \sigma}{\partial \xi} = \gamma_m = \frac{G_s + e}{1+e}\gamma_w \tag{3}$$

where σ is the total vertical stress, γ_m the current unit weight of saturated soil, G_s the specific gravity of the soil particle and γ_w the unit weight of water.

Based on the equilibrium of the pore water, we obtain

$$u_w = u_e + u_h \tag{4}$$

$$\frac{\partial u_w}{\partial \xi} = \frac{\partial u_e}{\partial \xi} + \gamma_w \tag{5}$$

where u_w is the total pore water pressure, u_e the excess pore water pressure and u_h the hydrostatic pressure.

Darcian law was initially observed from the seepage tests of sand, which have large interparticle voids. However, the Darcian law was not always applicable, particularly in fine grain soils (Miller and Low, 1963; Kutilek, 1964; Kutilek, 1972; Olsen, 1985). In fine soils, Non-Darcy's flow may occur due to the altered viscosity of pore water due to the influence of the soil's solid surface (Kutilek, 1964), the electrical streaming potential effect, osmosis because of chemical reactions such as those involved in aging effects (Olsen, 1985), or the change of the geometric arrangement of particles inside of the soil sample. Using a simplified non-Darcian flow relationship proposed by Indraratna et al. (2017) and taking into account the relative velocity of the fluid and solid phases in soil, we obtain

$$v = -ki^{\beta} \tag{6}$$

$$v = \frac{e}{1+e}\left(v_w - v_s\right) \tag{7}$$

$$\frac{e}{1+e}\left(v_w - v_s\right) = -k\left(\frac{1}{\gamma_w}\frac{\partial u_e}{\partial \xi}\right)^{\beta} \tag{8}$$

where v is the exit velocity, k the hydraulic conductivity, i the hydraulic gradient, β is a flow parameter, it should be noted that when β=0, Eq.(6) can degenerate into Darcy's law , and v_w and v_s the velocities of fluid and solid phases. Notably, the hydraulic conductivity k is a function of current void ratio e: $k = k(e)$.

As already mentioned, Lagrangian coordinates can simplify the solving of finite strain consolidation equations. Accordingly, general equations in Lagrangian coordinates will be developed.

The following formula has been shown to be satisfied in Lagrangian coordinates (Imai, 1995):

$$-\frac{1}{1+e_0}\frac{\partial e}{\partial t}=\frac{\partial v}{\partial a} \tag{9}$$

Incorporating Eqs.(6)–(8), Eq.(9) can rewritten as

$$\frac{\partial}{\partial a}\left[k\left(\frac{1}{\gamma_w}\frac{\partial u_e}{\partial \xi}\right)^{\beta}\right]=\frac{1}{1+e_0}\frac{\partial e}{\partial t} \tag{10}$$

Based on Eqs.(1) and (5), Eq.(10) can be absolutely expressed in Lagrangian coordinates as

$$\frac{\partial}{\partial a}\left[\frac{k}{\gamma_w^{\beta}}\left(\frac{1+e_0}{1+e}\frac{\partial u_w}{\partial a}-\gamma_w\right)^{\beta}\right]=\frac{1}{1+e_0}\frac{\partial e}{\partial t} \tag{11}$$

where t is the elapsed time.

Extension of Yin–Graham EVP model for finite strain

As already noted, few 1D finite strain consolidation theories has accounted for the creep of clayey soil slurry. This section introduces the 1D Yin–Graham EVP model and its modification for finite strain consolidation modelling. Bjerrum (1967) was among the first to investigate nonlinear time–dependent stress–strain in 1D oedometer conditions. Based on his work, Yin and Graham (1989, 1994) proposed and verified the 1D Yin–Graham EVP model for time–dependent behaviour of clays,

$$\dot{\varepsilon} = \frac{\kappa}{V}\frac{\dot{\sigma}'}{\sigma'} + \frac{\psi}{Vt_0}\exp\left[-\left(\varepsilon - \varepsilon_p^{ep}\right)\frac{V}{\psi}\right]\left(\frac{\sigma'}{\sigma_p'}\right)^{\lambda/\psi} \tag{12}$$

where ε and $\dot{\varepsilon}$ are the vertical strain and strain rate (compressive strain/stress is positive), σ' and $\dot{\sigma}'$ the vertical effective stress and stress rate, κ and λ the elastic and elastic–plastic compression index in Cam–clay models, t_0 and ψ the creep parameters, ε_p^{ep} the strain related to σ_p' and V the specific volume of the clay, with σ_p' having a role somewhat similar to that of pre–consolidation pressure p_c.

Eq.(12) is equivalent to

$$\dot{e} = -\kappa\frac{\dot{\sigma}'}{\sigma'} - \frac{\psi}{t_0}\exp\left(\frac{e - e_p^{ep}}{\psi}\right)\left(\frac{\sigma'}{\sigma_p'}\right)^{\lambda/\psi} \tag{13}$$

where e_p^{ep} is the void ratio related to σ_p'. σ_p' and e_p^{ep} together make a reference state point on the reference time line.

This study selects the 1D Yin-Graham EVP model, which is a representative creep model and equivalent to other kind of EVP models (Kutter and Sathialingam, 1992; Vermeer and

Neher, 1999; Yin et al., 2010). The 1D Yin–Graham EVP model can describe 1D stress or strain responses under general conditions, including multistage loading with creep straining, continuous loading and unloading or reloading. More importantly, the 1D Yin–Graham EVP model also belongs to Hypothesis B, assuming that creep contribution should be included throughout the consolidation and compression process. In addition, the model was widely adopted and verified by Yin and Graham (1996), Nash (2001), Nash and Ryde (2001), and Indraratna et al. (2018) to analyze the consolidation of soft soils with creep. However, for finite strain consolidation problems such as the self–weight consolidation of clayey slurry, the initial effective stress is small, even zero, and thus Eq.(12) is invalid because the strain will be infinite. In addition, as the deformation is negligible compared with soil thickness in finite strain problems, the relationship between vertical strain ε and current void ratio e exhibits two patterns: the first in convective coordinates,

$$\varepsilon_n = \ln\frac{1+e_0}{1+e} \tag{14}$$

where ε_n is called natural strain, and the second in Lagrangian coordinates,

$$\varepsilon_e = \frac{e_0 - e}{1+e_0} \tag{15}$$

where ε_e is called engineering strain. To avoid these two problems, the 1D Yin–Graham EVP model must be extended for the finite strain case, as elaborated in the follows.

Firstly, two logarithmic functions, for instant time line and reference time line, together with the creep equation used in the 1D Yin–Graham EVP model, are modified by introducing a non–zero small reference value σ'_{ref}, ranged from 0 to 1 kPa in the extended 1D EVP model.

For very soft soils with high water content, the initial value of σ' is close to 0 kPa. As shown in Eqs. (16)-(17), adding σ'_{ref} to the 1D Yin–Graham EVP model can keep strain from becoming too large or even infinite, which is particularly important for very soft clay in a soil ground with zero initial effective stress at the top of the surface. Secondly, the current 1D Yin–Graham EVP model is used mainly for small strain problems, meaning that there is no difference between using strain or void ratio to express the Yin–Graham model. For finite strain consolidation, the 1D Yin–Graham EVP model is better expressed using void ratio e as a variable instead of strain, to avoid inconsistency of strain expression. According to test data from Znidarcic et al. (1984, 1986) ($3 < e < 15$ for Florida Phosphatic Clay); Fox (1996) ($2 < e < 5$ for Southern Panther Creek Clay Slurry); Abu–Hejleh et al. (1996) ($3 < e < 13$ for Florida Phosphatic Clay); Sills (1998) ($1 < e < 6$ for Ketelmeer Mud); Stark et al. (2005) ($2 < e < 10$ for Georgia Inorganic Clay); and Pu et al. (2021) ($1 < e < 7$ for Stamford Harbor Sandy Clay), we know that void ratio e and logarithm of effective stress σ' show a nearly linear relation within a large range of void ratio e (see Figure 2), confirming the reasonableness of extending the 1D Yin–Graham EVP model to finite strain analyses.

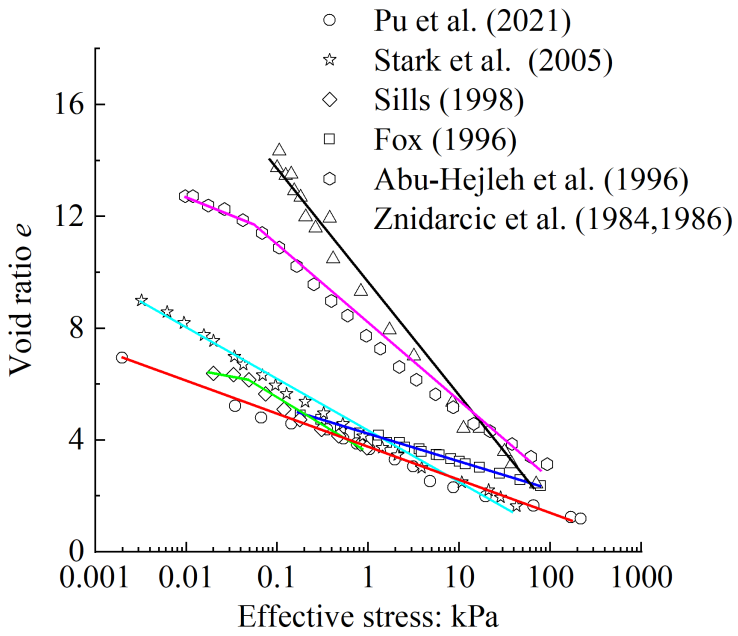

Figure 2–Void ratio–effective stress relationships of soil in high water content

Therefore, the modifications are expressed as

$$\Delta e^{e} = -\kappa \ln\left(\frac{\sigma'_{ref} + \sigma'}{\sigma'_{ref}}\right) \tag{16}$$

$$\Delta e^{ep} = -\lambda \ln\frac{\sigma'_{ref} + \sigma'}{\sigma'_{ref} + \sigma'_{p}} \tag{17}$$

$$\Delta e_{creep} = -\psi \ln\frac{t_0 + t_e}{t_0} \tag{18}$$

where σ'_{ref} is a reference non-zero small value, which can be taken as 0 to 1 kPa or checked by fitting test data at very small vertical effective stress, t_e the equivalent time in the 1D Yin–Graham EVP model.

Based on the above modifications, the 1D Yin–Graham EVP model is revised as the extended 1D EVP model for finite strain, as shown in Figure 3 and Eq.(19):

$$\dot{e} = -\kappa \frac{\dot{\sigma}'}{\sigma'_{ref} + \sigma'} - \frac{\psi}{t_0} \exp\left(\frac{e - e_p^{ep}}{\psi}\right)\left(\frac{\sigma'_{ref} + \sigma'}{\sigma'_{ref} + \sigma'_p}\right)^{\lambda/\psi} \tag{19}$$

The effective stress principle is expressed as

$$\sigma = \sigma' + u_w \tag{20}$$

Incorporating the effective stress principle, Eq.(19) could also be rewritten as

$$\frac{\partial e}{\partial t} = -\kappa \frac{\partial(\sigma - u_w)/\partial t}{\sigma'_{ref} + (\sigma - u_w)} - \frac{\psi}{t_0} \exp\left(\frac{e - e_p^{ep}}{\psi}\right)\left(\frac{\sigma'_{ref} + (\sigma - u_w)}{\sigma'_{ref} + \sigma'_p}\right)^{\lambda/\psi} \tag{21}$$

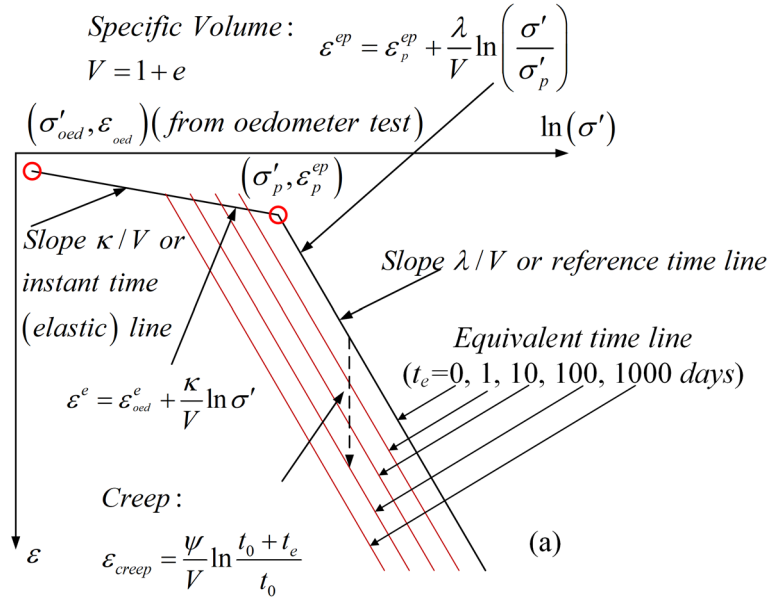

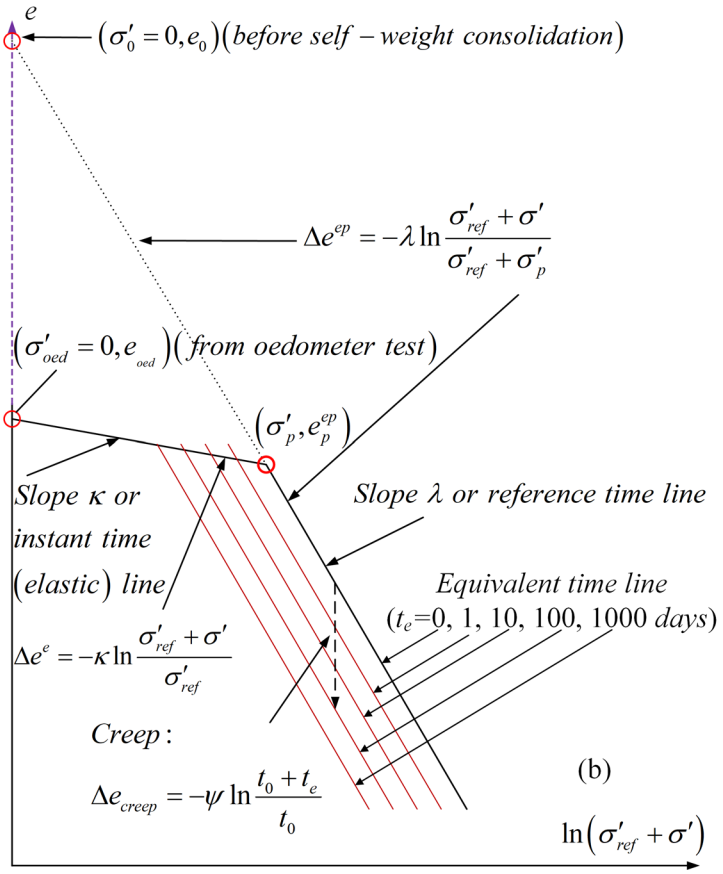

Figure 3–Existing 1D Yin–Graham EVP model and its extension for finite strain conditions: (a) Existing 1D Yin–Graham EVP model; (b) Extended 1D Yin–Graham EVP model for finite strain conditions

Extension of 1D finite strain consolidation considering creep

Equations (3), (11), and (21) can be used to solve for the three unknowns e, u_w and σ. Vertical strain ε, vertical settlement S, excess pore pressure u_e and vertical effective stress σ' can be readily calculated from the values of e, u_w and σ as rewritten in Eqs.(22)-(24) in Lagrangian coordinates

$$\frac{\partial \sigma}{\partial a} = \frac{G_s + e}{1 + e_0} \gamma_w \tag{22}$$

$$\frac{\partial}{\partial a}\left[\frac{k}{\gamma_w^{\beta}} \left(\frac{1 + e_0}{1 + e} \frac{\partial u_w}{\partial a} - \gamma_w \right)^{\beta} \right] = -m_v \frac{\partial (\sigma - u_w)}{\partial t} - g(u_w, e, \sigma) \tag{23}$$

$$\frac{1}{1+e_0}\frac{\partial e}{\partial t}=-m_v\frac{\partial\left(\sigma-u_w\right)}{\partial t}-g\left(u_w,e,\sigma\right) \tag{24}$$

where

$$m_v=\frac{\kappa/\left(1+e_0\right)}{\sigma'_{ref}+\left(\sigma-u_w\right)} \tag{25}$$

$$g\left(u,e,\sigma\right)=\frac{\psi}{\left(1+e_0\right)t_0}\exp\left(\frac{e-e_p^{ep}}{\psi}\right)\left[\frac{\sigma'_{ref}+\left(\sigma-u_w\right)}{\sigma'_{ref}+\sigma'_p}\right]^{\lambda/\psi} \tag{26}$$

Observing that $(1 + e)$ occurs in the present finite strain consolidation equations, we choose an empirical power function equation used by Zeng et al. (2020), Wang et al. (2020), and Winterwerp (1999) for quantitatively describing k, expressed as

$$k=k_0\left(1+e\right)^n \tag{27}$$

where k_0 and n are empirical coefficients. This expression is not only the same in nature as the expression of $k=C(\boldsymbol{e})^D$, which has well modelled the permeability for clay with both high and low water content (Pane and Schiffman, 1997; Berilgen et al., 2006; Dolinar, 2009), but also inherits the advantages of the expression of $k = k_0(1 + e)$ used by Been and Sills (1981), making it helpful for simplifying the consolidation equations by eliminating separate $(1 + e)$ terms.

We usually want to obtain the excess pore water pressure u_e directly, so here we introduce

$$\sigma=\sigma_{ah}+u_h \tag{28}$$

where σ_{ah} is the total stress above hydrostatic pressure.

Also, combining Eqs.(4), (20), and (28), we can express effective stress by

$$\sigma'=\sigma_{ah}-u_e \tag{29}$$

Using u_e, σ_{ah} instead of u_w, σ respectively, Eqs.(22)–(26) could be rewritten as

$$\frac{\partial \sigma_{ah}}{\partial a} = \frac{G_s - 1}{1 + e_0} \gamma_w \tag{30}$$

$$\frac{\partial}{\partial a}\left[\frac{k}{\gamma_w^{\beta}} \left(\frac{1 + e_0}{1 + e} \frac{\partial u_e}{\partial a} \right)^{\beta} \right] = -m_v \frac{\partial \left(\sigma_{ah} - u_e \right)}{\partial t} - g\left(u_e, e, \sigma_{ah} \right) \tag{31}$$

$$\frac{1}{1 + e_0} \frac{\partial e}{\partial t} = m_v \frac{\partial u_e}{\partial t} - g\left(u_e, e, \sigma_{ah} \right) \tag{32}$$

where

$$m_v = \frac{\kappa / \left(1 + e_0 \right)}{\sigma'_{ref} + \left(\sigma_{ah} - u_e \right)} \tag{33}$$

$$g\left(u_e, e, \sigma_{ah} \right) = \frac{\psi}{\left(1 + e_0 \right) t_0} \exp\left(\frac{e - e_p^{ep}}{\psi} \right) \left(\frac{\sigma'_{ref} + \left(\sigma_{ah} - u_e \right)}{\sigma'_{ref} + \sigma'_p} \right)^{\lambda / \psi} \tag{34}$$

which is to say that Eqs.(22)–(26) or Eqs.(30)–(34) formulate a 1D finite strain consolidation theory that takes into account soil creep. It should be noted that permeability k is expressed by Eq.(27).

Note that the above modifications and derivations are also applicable to other elastic visco-plastic models of soft clays (e.g. Stolle et al., 1999; Kim and Leroueil, 2001; Yin and Wang, 2012). Imai (1981) summarized that the slurry in a settling column experiences three stages: flocculation stage, settling stage, and consolidation stage. The proposed consolidation model of this study is to capture the settling of soil particles already with inter-particle contact forces and self-weight consolidation behaviour in the last two stages since the effective stress begins to develop. In addition, it also should be noted that the proposed finite strain

consolidation model can capture the creep characteristics of clayey soil once the consolidation process started no matter how long or how short the process of self-weight consolidation.

Finite difference method–based solution

The proposed 1D finite strain consolidation model with consideration of creep for clayey soil consists of a set of highly nonlinear partial differential equations. Yin and Graham (1996) and Zhu and Yin (1999) used the finite difference method and finite element method to solve a set of nonlinear partial differential equations. In this section, the Crank–Nicholson finite difference program, much as in Yin and Graham (1996), is formulated to solve Eqs.(30)–(34) due to its good stability and accuracy. The Crank–Nicolson finite difference method combines the forward Euler and the backward Euler methods. The central difference is used in space to reduce the calculation error.

Performing the difference in time and space, as shown in Figure 4, for Eqs.(30)–(32), we obtain

$$\left(\sigma_{ah}\right)_{i+1,j}=\left(G_s-1\right)/\left(1+e_0\right)\gamma_w\Delta a+\left(\sigma_{ah}\right)_{i,j} \tag{35}$$

$$A_{i,j}u_{i-1,j+1}-\left(2A_{i,j}+1\right)u_{i,j+1}+A_{i,j}u_{i+1,j+1}=\left(2A_{i,j}-1\right)u_{i,j}-\left(A_{i,j}+B_{i,j}\right)u_{i+1,j}+\left(B_{i,j}-A_{i,j}\right)u_{i-1,j}-C_{i,j} \tag{36}$$

$$e_{i,j+1}=\left\{\left(m_v\right)_{i,j}\times\left(u_{i,j+1}-u_{i,j}\right)-\Delta t\times\left[g\left(u_e,e,\sigma_{ah}\right)\right]_{i,j}\right\}\times\left(1+e_0\right)+e_{i,j} \tag{37}$$

where the subscripts i (0, 1, …, N) represent variation in depth, described by the a coordinate, and the subscripts j (0, 1, …, M) represent variation in the time t coordinate, with $A_{i,j}=r_{i,j}\beta\left(1+e\right)_{i,j}$, $B_{i,j}=r_{i,j}\left(n-\beta\right)\left(e_{i+1,j}-e_{i,j}\right)$, $C_{i,j}=\Delta t\left[g\left(u_e,e,\sigma_{ah}\right)/m_v\right]_{i,j}$,

287 $r_{i,j} = \left(C_v\right)_{i,j} \dfrac{\Delta t}{2\left(\Delta a\right)^2}$, and $C_v = \dfrac{k_0\left(1+e_0\right)^{\beta}\left(1+e\right)^{n-\beta-1}}{\gamma_w^{\beta}}\left(\dfrac{\partial u_e}{\partial a}\right)^{\beta-1}$. The depth increment

288 $\Delta a = a_{i+1} - a_i$ has been kept constant, but the time increment $\Delta t = t_{j+1} - t_j$ has been allowed to

289 increase with the development of consolidation for good convergence in the early stage of the

290 consolidation, as well as quicker calculation in the later stage.

291 Figure 4 also shows the boundaries in Lagrangian coordinates. The initial thickness of the

292 soil layer is a_0. Assuming that the top of the soil layer (a = 0) is freely draining, the pore water

293 pressure u_w will be constant and the excess pore water pressure u_e will be zero. At the bottom

294 of the soil, we consider an undrained condition that can be expressed by $\partial u_e / \partial a = 0$. The

295 complex drainage boundaries (e.g., Mei et al., 2022; Feng et al., 2020; Feng et al.,2019; Mei et

296 al., 2014) are not considered here. Because the effective stress is zero at the top of the soil layer

297 during the process, the initial void ratio at a = 0 is $e = e_0$. These boundaries can be expressed

298 in a finite difference form:

299 $$\left(u_e\right)_{0,j} = 0 \ \left(\text{where } j=0, 1, 2, 3, \ldots, M\right) \tag{38}$$

300 $$\left(u_e\right)_{n,j} - \left(u_e\right)_{n-1,j} = 0 \ \left(\text{where } j=0, 1, 2, 3, \ldots, M\right) \tag{39}$$

301 $$\left(e\right)_{0,j} = e_0 \ \left(\text{where } j=0, 1, 2, 3, \ldots, M\right) \tag{40}$$

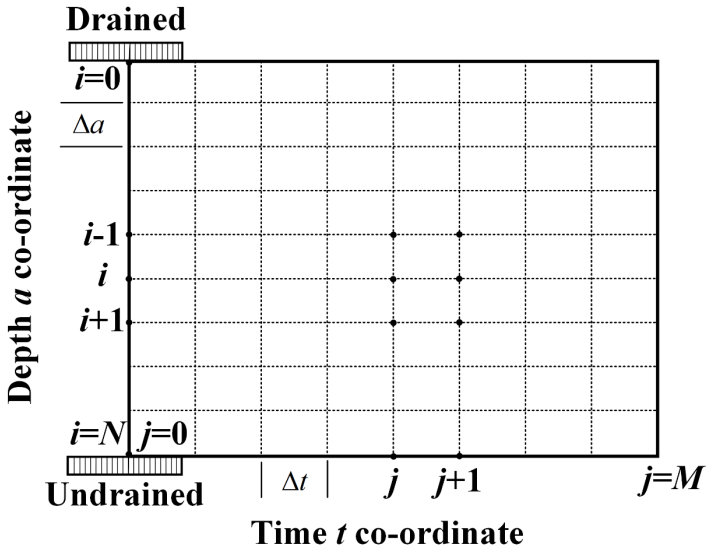

302

303 Figure 4–Finite difference grid and boundaries

304 Settlement can be calculated as

305 $$S = \int_0^a \left(\frac{e - e_0}{1 + e_0} \right) da \tag{41}$$

306 An approximate numerical solution of Eq.(41) can be written

307 $$S_j = \left[0.5 \left(\frac{e - e_0}{1 + e_0} \right)_{0,j} + 0.5 \left(\frac{e - e_0}{1 + e_0} \right)_{n,j} + \sum_{i=1}^{n-1} \left(\frac{e - e_0}{1 + e_0} \right)_{i,j} \right] \Delta a \tag{42}$$

308 For the case of self–weight consolidation, initial consolidation excess pore water
309 distributes linearly along the height of soil column and the effective stress is zero. By
310 combining equations (29) and (30), the initial excess pore water pressure is obtained, which
311 distributes linearly along the height of soil column with the constant slope of $(G_s\text{-}1)\gamma_w/(1+e_0)$.
312 The distribution can be expressed as a function of depth as follow:

313 $$u_e(a,0) = \frac{(G_s - 1)}{(1 + e_0)} \gamma_w a \tag{43}$$

The proposed consolidation model was rigorously derived. Therefore, it is suitable for simulating the consolidation process with surcharge or fill. The surcharge can be time-dependent or constant, which can be applied through adjusting the total stress expression. Further, the numerical algorithm follows the Crank–Nicholson finite difference method which is flexible in setting the boundary and initial conditions. The proposed model can also be used to describe the case of double-sided drainage by adjusting the boundary conditions (e.g., Eqs. (38) and (39)). It is convenient to set the initial conditions by giving different void ratios or initial stress to simulate the case with a non-uniform void or stress distribution.

Application in self–weight consolidation case studies

Many setting columns have been used to research setting and consolidation behaviour. Been and Sills (1981) was the first to set a series of laboratory model tests of the development and consolidation of soft soil in settling columns, with measurement of density (using an accurate, non–destructive X–ray technique), total stress, pore pressure and surface settlement. A workshop "Sidere" was held in Oxford in 2000, in which four self–weight tests were carried out and the four of the test results were presented to participants for them to predict the results of the fifth experiment for which only the initial condition was known (Barhtolomeeusen et al., 2002). Alexis et al. (2004) provided a more accurate follow–up on densities and interstitial excess pore pressures. Bonin et al. (2014) presented a detailed examination of thickened tailings undergoing self–weight consolidation and a slurry consolidometer obtaining the compressibility relationship under low vertical effective stresses.

In this paper, the Experiment 15 reported by Been and Sills (1981) and Sidc 1 and Sidc 3 reported by Barhtolomeeusen et al. (2002), here called Case 1 and Case 2, respectively, were

chosen to verify proposed 1D finite strain theory for self–weight consolidation with creep. Case 1 used a larger initial void ratio than Case 2. In addition, Case 1 consisted of only Class C prediction, while Case 2 included both Class C and Class A predictions, with Class A prediction defined as the prediction made before construction based entirely on data available at that time, and Class C made after the occurrence of the event being predicted (Lambe, 1973). For simplicity, it is assumed that the flow of water in all case studies follows Darcy's law, i.e. $\beta = 1$.

Case Study 1

Experiment 15 reported by Been and Sills (1981) was chosen as Case 1 to verify the proposed 1D finite strain theory for two reasons: (1) more detailed data were provided than in other consolidation experiments, and (2) the setting column in this experiment underwent less settling suspension and self–weight consolidation from a state with high water content and a large void ratio. In Case 1, a natural soil from the River Parrett estuary was used that has a liquid limit (w_L) of 53%, plastic limit (w_P) of 25%, plasticity index (I_P) of 28%, and specific gravity of 2.66. The clay content (CI) of the soil is approximately 30%. The initial height and unit weight of the soil column are 0.643 m and 11.2 kN/m^3, respectively. Further details of Case 1 are presented and discussed in Been (1980) and Been and Sills (1981).

All parameters in current 1D finite strain theory should have been determined by using the detailed procedure proposed by Yin and Graham (1994), according to the oedometer test data. For the extremely soft soil with high initial water content, Hong et al. (2010) modified the conventional oedometer apparatus using a light loading cap and two weight hangers system which can be used to perform tests on the soil with initial water content that is double of liquid limit allowing a small load (e.g. 0.5 kPa). Furthermore, Xu et al. (2015) improved the

conventional oedometer apparatus by a leverage for the soil sample with high initial water content to 4.4 times of the liquid limit allowing a small load (e.g. 0.1 kPa). For clay with water content higher than 4.4 times of its liquid limit, the settling column test is an effective method to investigate the compression behaviour with very high void ratio and very small effective stress. However, due to the absence of oedometer test data for the soil used in Been and Sills (1981), a simple approximation method for determining all parameters of the 1D finite strain theory is proposed.

Firstly, the reference stress σ'_{ref} can be obtained from stress–strain curves of Experiment 15 (Fig. 13, Been and Sills, 1981). Herein, by fitting the test data at the range of small effective stress (Been and Sills, 1981; Znidarcic et al. 1984, 1986; Fox, 1996; Barhtolomeeusen et al., 2002; Abu–Hejleh et al., 1996; Sills, 1998; Stark et al., 2005, Pu et al., 2021), an exponential relationship between the initial void ratio e_0 and the reference stress σ'_{ref} is assumed:

$$\sigma'_{ref} = 0.0193\exp\left(-0.3e_0\right) \tag{44}$$

The Eq.(44) shows higher void ratio gives smaller reference effective stress, which is reasonable.

The compression index C_c can then be obtained by drawing a best–fit line through the stress–strain data of Experiment 15 (Fig. 13, Been and Sills, 1981). The ratio between unloading–reloading compression index C_r and compression index C_c is approximately 1/5 ~ 1/10 by many researchers, and $C_r = C_c/6$ is adopted in this paper. The most straightforward method of obtaining the creep index is by laboratory tests. However, we usually

379 did not have detailed test data to get it. Therefore, the practical methods of determining the
380 creep index are summarized to provide helpful reference for the corresponding application.
381 One approach is using the empirical formula for the creep coefficient based on physical
382 parameters of soils (Zhang et al., 2020; Jin et al., 2019; Yin, 1999). Another simple method is
383 to calculate the creep index C_α by a typical ratio of creep index C_α to the compression index
384 C_c based on soil classification and components (Mesri and Castro, 1987; Mitchell and Soga,
385 2005). The creep index C_α is obtained using the recently proposed correlation (Jin et al., 2019)

386 $$\ln\left(C_\alpha\right)=\left(0.3114\frac{I_p^2}{CI}-0.1229\frac{1}{I_p^2}+0.6455\frac{1}{I_p}\right)e-5.1308 \tag{45}$$

387 where I_p is the plasticity index and CI the clay content.

388 According to Yin and Zhu (2020), we can calculate current 1D finite consolidation model
389 parameters κ, λ, ψ and t_0 using the approximate relationships

390 $$\begin{cases}\kappa\approx\dfrac{C_r}{\ln(10)} \quad \lambda\approx\dfrac{C_c}{\ln(10)} \quad \psi\approx\dfrac{C_\alpha}{\ln(10)} \\ t_0=1440\,\text{min}\end{cases} \tag{46}$$

391 The parameter t_0 is chosen as 1400 min or 1 day corresponding to a loading duration of
392 conventional oedometer test, which is also widely adopted in other creep models (e.g. Kutter
393 and Sathialingam, 1992; Leoni et al., 2008; Yin et al., 2010). It is a relatively simple and
394 practically useful way. Using Eq.(27) to draw a best–fit line through the permeability profiles
395 of Experiment 15 (Fig. 15, Been and Sills, 1981), the relationship between permeability and
396 void ratio can be expressed by $k=1.38\times10^{-10}\left(1+e\right)^{4.03}$. Finally, e_{oed} = 1.5 is assumed, where
397 the e_{oed} is the initial void ratio of the soil sample, which is used to obtain the point $\left(\sigma_p',e_p^{ep}\right)$ in

398 the reference time line in Figure 3(*b*). All the parameters of current 1D finite strain theory are
399 obtained from Experiment 15 (Been and Sills, 1981) as shown in Table 1.

400 Table 1 Compression and consolidation parameters used in the case studies

Parameters	Case Study 1 (Been and Sills, 1981)	Case Study 2 (Barhtolomeeusen et al., 2002)	
	Experiment 15,	Sidc 1	Sidc 3
e_0	9.87	2.48	2.09
λ	1.02	0.2	0.15
I_P	28%	11%	11%
CI	30%	10%	10%
t_0 / min	1440	1440	1440
σ'_p / kPa	8.70	0.99	1.65
k_0 / (m / s)	1.38×10^{-10}	8.85×10^{-12}	5.59×10^{-12}
n	4.0	9.7	10.6

401 As proposed in Carrier et al. (1983), Sills (1998) and Stark et al. (2005), consolidation
402 occurs only when a continuous soil structure is developed. The corresponding void ratio and
403 density are called initial void ratio and structural density, respectively. According to Carrier et
404 al. (1983), the initial void ratio used to distinguish the end of sedimentation and the beginning
405 of consolidation can be obtained using the correlation $e_0 = 0.07G_s(100w_L)$. The initial void
406 ratio of Experiment 15 (Been and Sills, 1981) determined by the preceding correlation is 9.87
407 (7.5 times the void ratio at the liquid limit), and the corresponding structural density of soil is
408 11.3 kN/m^3, which is higher than the initial density, 11.2 kN/m^3, of soil in Experiment 15 (Been
409 and Sills, 1981). Thus soil consolidation did not start at the beginning of the experiment, and a
410 little settling suspension was seen.

411 In Experiment 15 (Been and Sills, 1981), the top of the soil column ($a = 0$) is permeable
412 and the bottom of soil column ($a = a_0$) impermeable. Accordingly, the boundary conditions can
413 be simply stated mathematically with respect to excess pore water pressure u_e as

414 $$u_e(0,\ t) = 0 \tag{47}$$

415 $$\frac{\partial u_e}{\partial a}(a_0,\ t) = 0 \tag{48}$$

416 At the beginning of self–weight consolidation, the initial excess pore water pressure
417 distribution can be obtained from Eq.(43):

418 $$u_e(a, 0) = 1.497a \tag{49}$$

419 To verify the accuracy of current 1D finite strain theory, Case 1 is reproduced using the
420 Crank–Nicholson finite difference program already proposed. The predicted surface settlement,
421 total stress, excess pore water pressure, void ratio and density profiles are obtained.

422 Figure 5 shows the predicted and measured surface settlement of Case 1 at different
423 periods. It can be seen that the predicted settlement under current 1D finite strain theory
424 captures the progress of self–weight consolidation in the experiment and the surface settlement
425 profile quite well.

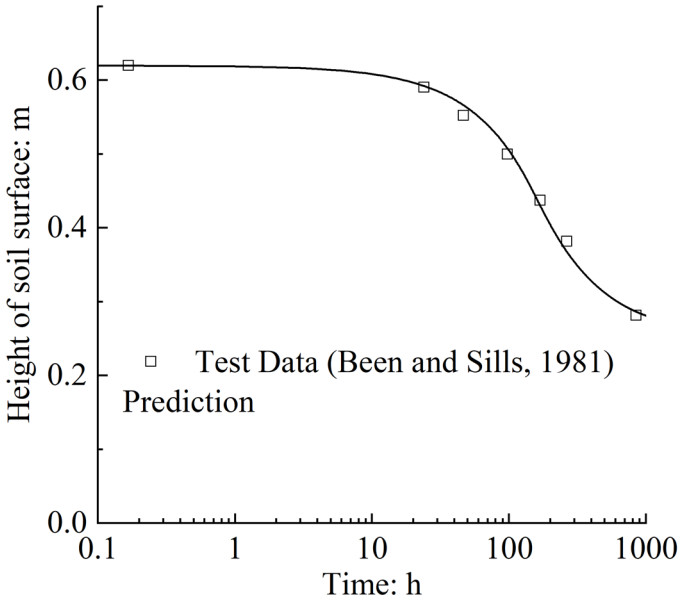

426

427 Figure 5–Predicted and measured settlement, experiment 15 (Been and Sills, 1981)

428 The settlement profile is highly significant in reclamation projects, but the density profile
429 and pore pressure dissipation process are also of great interest in a riverbed design and
430 resuspension of mine tailings, because the strength of a soil bed depends on the effective stress
431 and void ratio – that is, successful modelling of the self–weight consolidation process must
432 include prediction of not only surface settlement but also excess pore pressure and void ratio
433 profile. Figure 6 and Figure 7 show the excess pore water pressure and total stress profiles
434 determined from the finite strain modelling and observed in Case 1. According to Figure 6, the
435 excess pore water pressure distributed linearly along the height of the soil column at the
436 beginning of the consolidation process and the slope is $(G_s - 1)\gamma_w / (1 + e_0)$. With time, the
437 excess pore water pressure gradually dissipates upwards from the bottom of the soil column, a
438 phenomenon also observed by Bartholomeeusen et al. (2002) and Bonin et al. (2014). The
439 excess pore water pressure distributes linearly along the depth. The maximum excess pore

water pressure is in the bottom of the soil column. The predictions concerning the excess pore water pressure dissipation process by the finite strain model agree well with the measured data, confirming the reliability of the finite strain theory. Figure 7 also verifies that the current 1D finite strain theory simulates the total stress on the soil column base in the consolidation process well. Based on Figure 7, the total stress of the column base is unchanged during the self–weight consolidation process, with no water or soil discharged during the whole experiment, and thus agrees well with the phenomenon observed in the experiment.

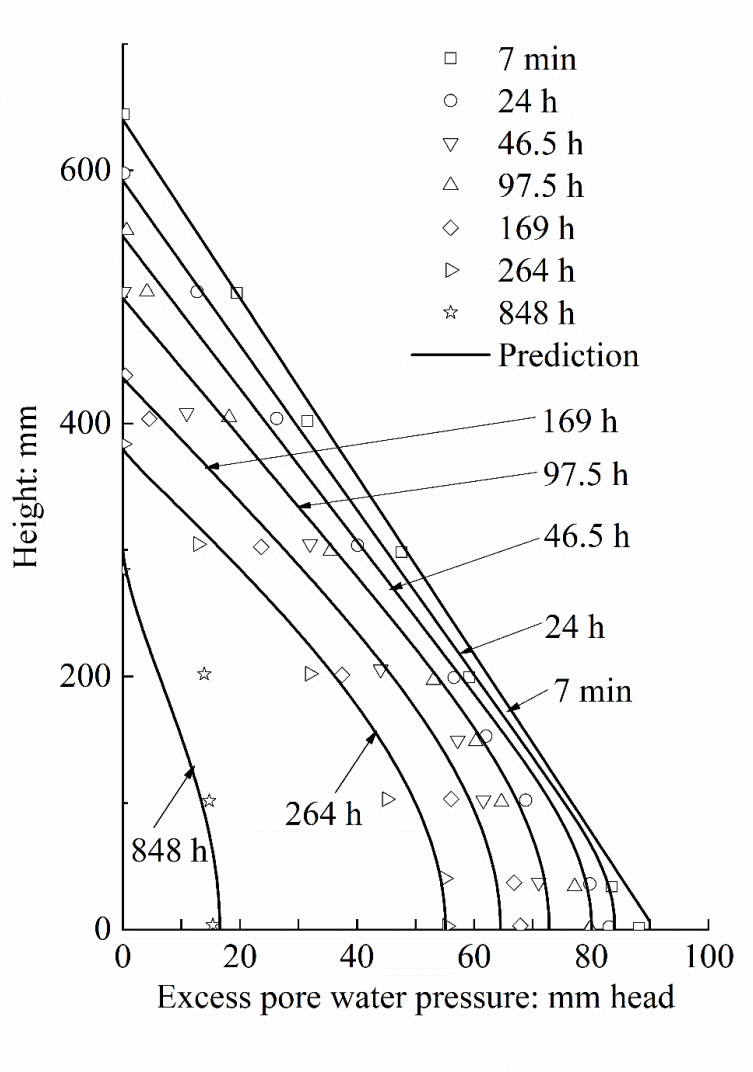

Figure 6–Predicted and measured excess pore water pressure, experiment 15 (Been and Sills, 1981)

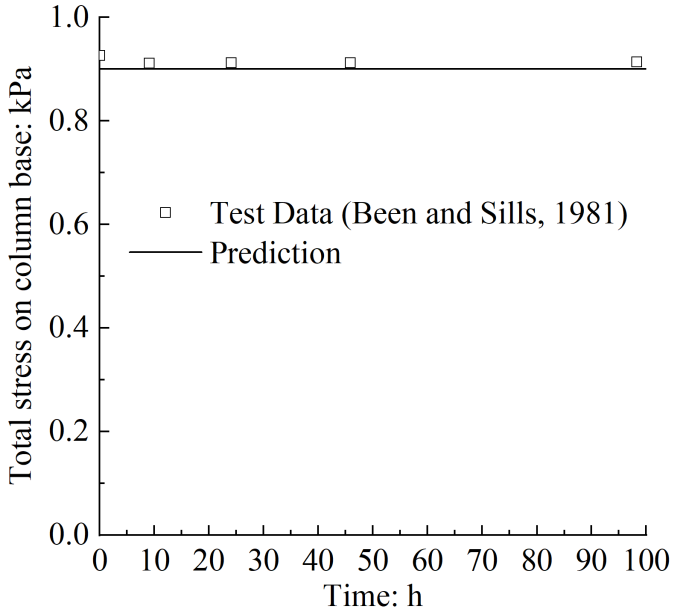

449

450 Figure 7–Predicted and experimental total stress on column base, experiment 15 (Been and Sills, 1981)

451 In addition, Figure 8 shows a comparison between the measured and predicted void ratio
452 distribution with the consolidation process, which is equivalent to the density profile (Figure
453 9). Based on the void ratio distribution time and space, self–weight consolidation can cause
454 redistribution of the void ratio along the soil column height. In the self–weight consolidation
455 process, the void ratio of the soil column base decreases firstly and the other portion stays at
456 the initial void ratio unless the self–weight consolidation begins. Theoretically speaking, this
457 phenomenon is reasonable. The above evolution of void ratio in the self-weight consolidation
458 process is consistent with the results reported by Pu et al. (2018) and Bonin et al. (2014). There
459 is discrepancy that measured void ratios at different positions in the soil column did not keep
460 constant at the early consolidation stage as predicted, which can be possibly explained as
461 follows: (1) the existing inhomogeneity of the dredged mud in the experiment was ignored in
462 the simulation where the initial void ratio of the whole soil column was assumed homogenous,

as reported by Been and Sills (1981); (2) the experimental stress and strain curves provided by Been and Sills (1981) are dispersal, leading to inaccurate model parameters. Under a high initial void ratio, a small change of effective stress may correspond to a big change of void ratio, which may also cause the deviation between the predicted and experimental values. It should be noted, however, that the predicted density file is somewhat different from that observed during the early stages of self–consolidation, especially near the bottom of the soil column. However, as self–consolidation develops, the predicted and measured densities show better agreement, possibly because the soil sample used in the self–weight experiment was taken from natural soil. During the early stages of self–consolidation, the density distribution is less uniform compared with its state when the structure of the soil layer increases. Overall, all prediction profiles confirm the reliability of the finite strain theory proposed in this paper for simulating self–consolidation of soft soil.

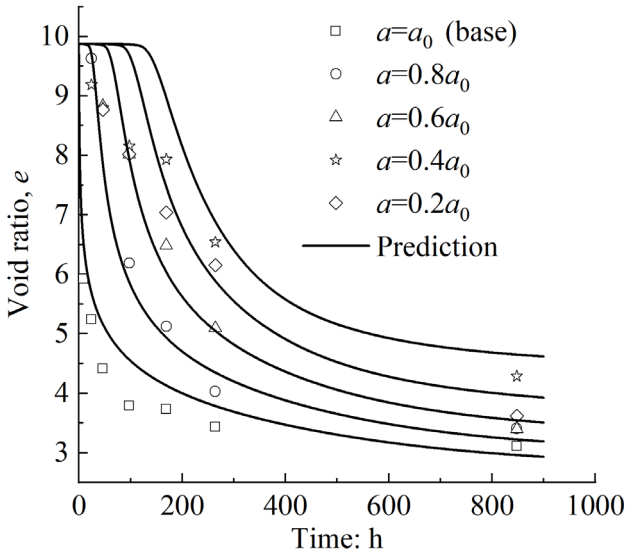

Figure 8–Comparison between predicted and experimental void ratio, experiment 15 (Been and Sills, 1981)

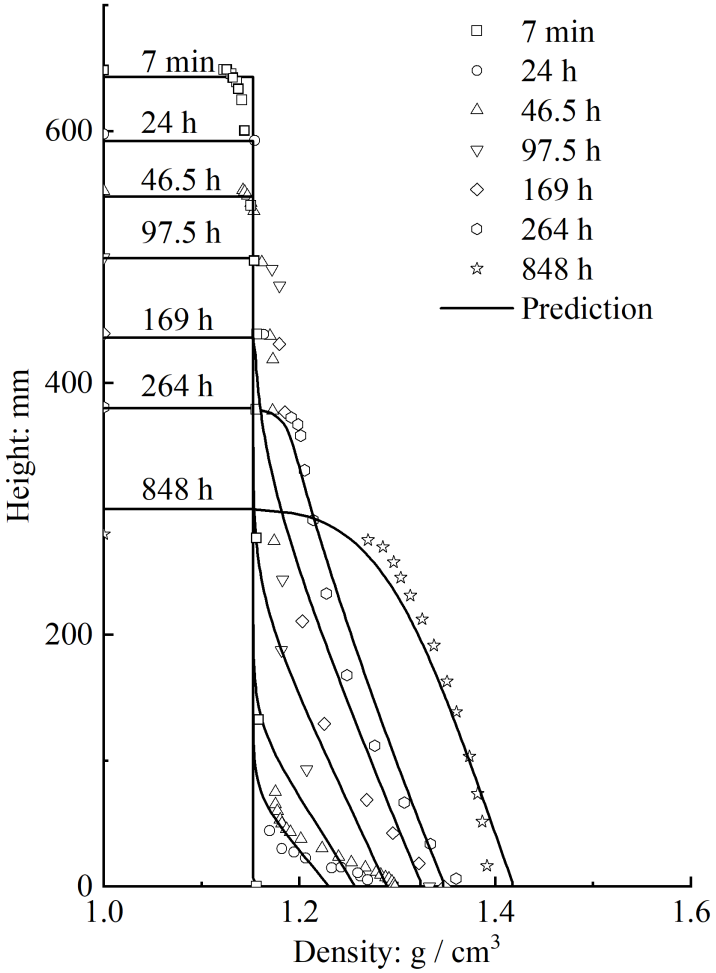

478

479 Figure 9–Predicted and measured density, experiment 15 (Been and Sills, 1981)

480 Furthermore, the comparison between the measured and predicted settlement and excess
481 pore water pressure with and without considering creep was also conducted. From Figure 10,
482 it can be seen that the predicted settlement with creep is almost consistent with that without
483 considering creep within the first 200 h. However, the deviation of settlement curve with and
484 without creep begins to appear after 200 h. The difference becomes larger with time going by.
485 It also should be noted that the simulation with creep better captures the development trend of
486 settlement in the monitoring period than that without considering creep. The predicted

settlement without considering creep is kept stable after about 1000 h, which underestimates the settlement. Figure 11 shows the excess pore water pressures predicted using the proposed model with and without the creep. The dissipation rate of excess pore water pressure is found overestimated if the creep of clay is not considered which is consistent with the analysis reported by Liu et al. (2018) and Indraratna et al. (2018). This phenomenon may be due to the deformation caused by soil creep, which reduces the dissipation of pore water when the same settlement occurs.

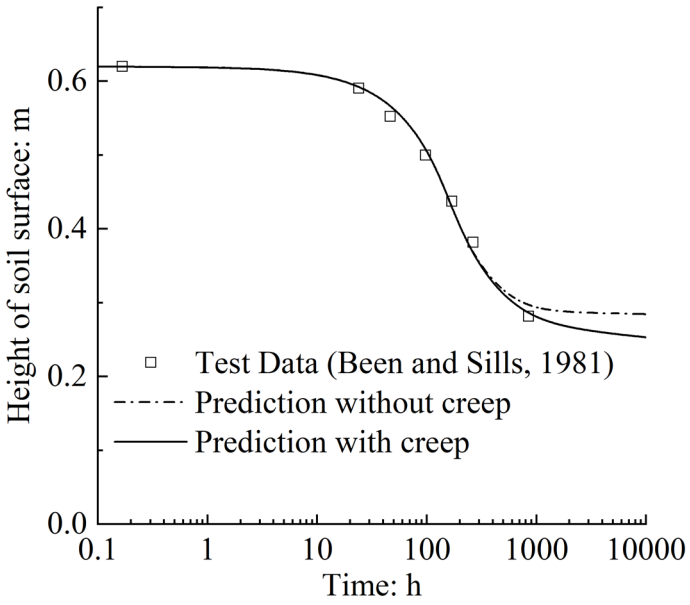

Figure 10–Comparison between measured and calculated settlements with and without considering creep for the experiment 15 of Been and Sills (1981)

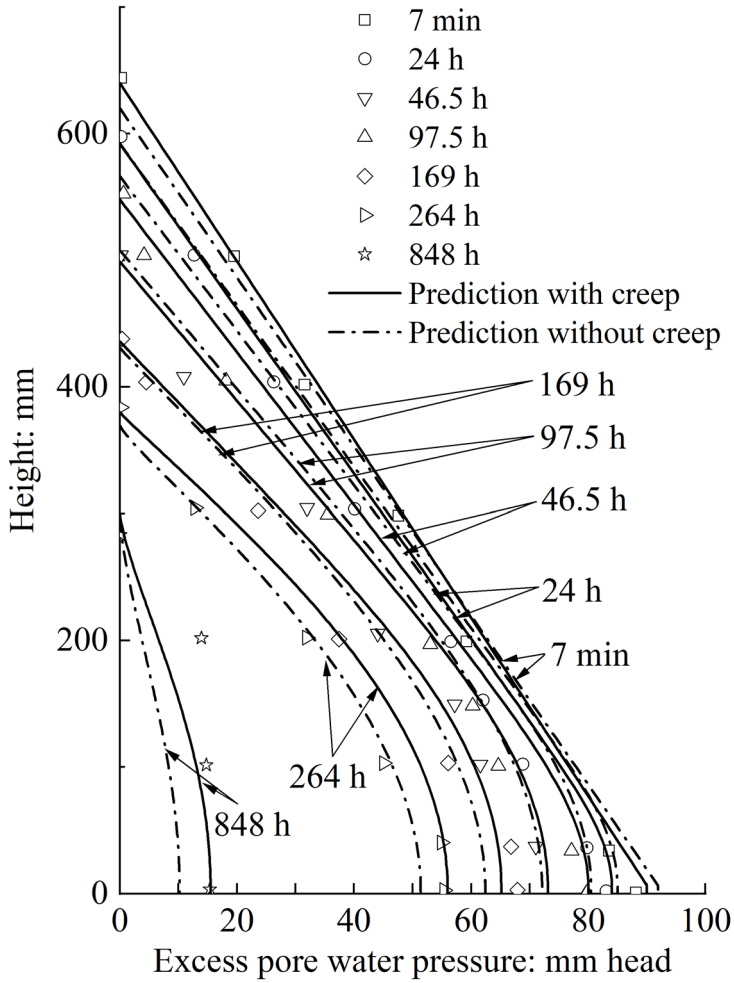

497

498 Figure 11–Comparison between measured and calculated excess pore water pressures with and without

499 considering creep for the experiment 15 of Been and Sills (1981)

500 **Case Study 2**

501 Sidc1 and Sidc3, reported by Bartholomeeusen et al. (2002), were chosen as Case 2 to
502 verify the reliability when the initial void ratio (2 times void ratio at the liquid limit) is relatively
503 smaller than in Case 1 (7.5 times void ratio at the liquid limit). In addition, Case 2 consisted of
504 not only Class A but also Class C prediction and has been simulated by many researchers, such
505 as Hawlader et al. (2008), whose prediction results are compared with those by other
506 researchers. In Case 2, the soil was collected from the river Schelde in Antwerpen, which has

507 a liquid limit of 39%, plastic limit of 28%, plasticity index of 11%, and specific gravity of 2.72.
508 The clay content of the soil is less than 10%.The boundary conditions of Case 2 are the same
509 as in Case 1. Further details of Case 2 are presented and discussed in Bartholomeeusen et al.
510 (2002). The method used to determine the parameters in current 1D finite strain theory is the
511 same as in Case Study 1 and the parameters are shown in Table 1.

512 Hawlader et al. (2008) developed a state–dependent model of the compressibility
513 behaviour of soft clay sediments at a low effective stress level, which can capture the feature
514 whereby stress–strain relationships are not unique but rather depend on the state of the element
515 concerning its location (Been and Sills, 1981; Bartholomeeusen et al., 2002). However, the
516 constitutive model proposed by Hawlader et al. (2008) is a complete empirical formula and is
517 not related to the conventional compressibility indexes. Because the time required to attain the
518 same effective stress through pore water pressure dissipation differs for soil elements along the
519 depth, Been and Sills (1981) and Sills (1995) have attributed differences in the stress–strain
520 relationships of different locations to creep of clayey soil. Accordingly, Case 2 is used to verify
521 that present model can also simulate the self–weight consolidation well, even better than
522 described in Hawlader et al. (2008), by considering the creep of clayey soil.

523 Figure 12 compares the predicted surface settlement by the proposed model and Hawlader
524 et al. (2008) and measured surface settlement for Case 2, showing that the predicted settlement
525 under both current 1D finite strain theory and Hawlader can capture the surface settlement
526 profile of Sidc 3 in Case 2 quite well. However, for the Class C prediction, Sidc 1, Hawlader
527 et al. (2008) clearly overestimated the settlement, predicting that the majority of the settlement
528 would be almost completed after 7 days. But the present model prediction results indicate that

529 settlement of Sidc 1 is still on–going at 7 days, as the experiment showed. Thus the present
530 model's prediction of settlement during the self–weight consolidation process (small effective
531 stress range) equals or exceeds Hawlader et al. (2008)'s results.

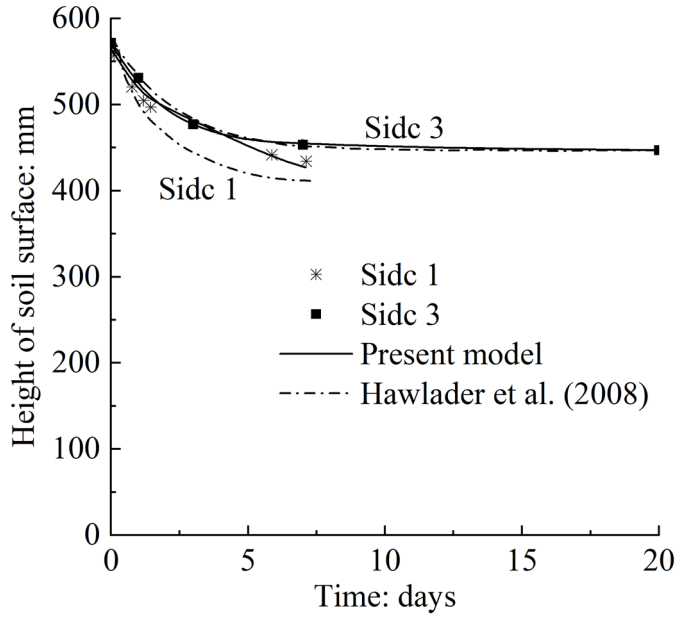

532

533 Figure 12–Predicted and measured settlement, Sidc 1 and Sidc 3 (Barhtolomeeusen et al., 2002; Hawlader
534 et al., 2008)

535 Figure 13 compares the measured and predicted excess pore water pressure distribution
536 during the consolidation process, showing that the settlement predicted by both current 1D
537 finite strain theory and Hawlader et al. (2008) reflects the surface settlement profile of Sidc 3
538 in Case 2 quite well during early stages 0–1 d. However, as self–weight consolidation time
539 lengthened, Hawlader et al. (2008) predicted quicker excess pore water pressure dissipation
540 process than seen in experimental observations. Current 1D finite strain theory thus simulated
541 the excess pore water pressure dissipation process better.

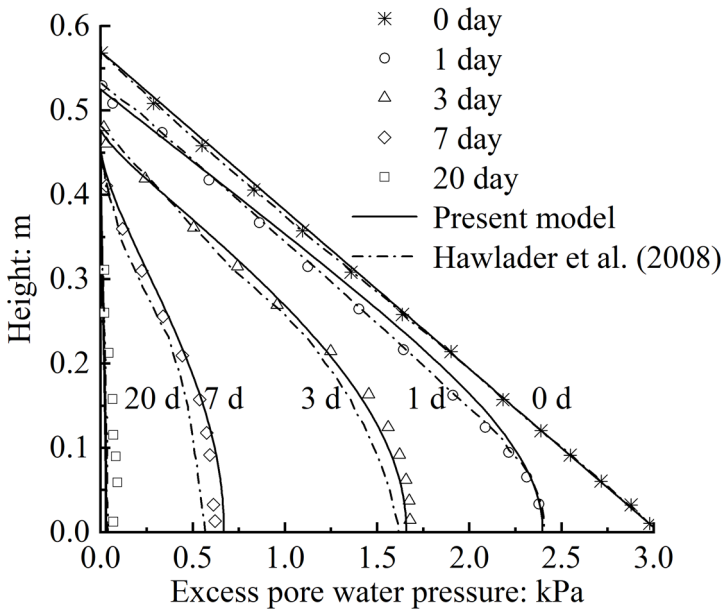

542

543 Figure 13–Predicted and measured excess pore water pressure, Sidc 3 (Barhtolomeeusen et al., 2002;

544 Hawlader et al., 2008)

545 Figure 14 compares the measured and predicted density distribution during the
546 consolidation process, indicating that the density distribution predicted by the present model
547 was better than the prediction made by Hawlader et al. (2008) in the bottom zone but worse in
548 the top zone, where the effective stress is relatively small. This phenomenon occurs because
549 the state–dependent constitutive model proposed by Hawlader et al. (2008) can describe the
550 stress–strain relationship better than the current model in the extreme effective stress range.

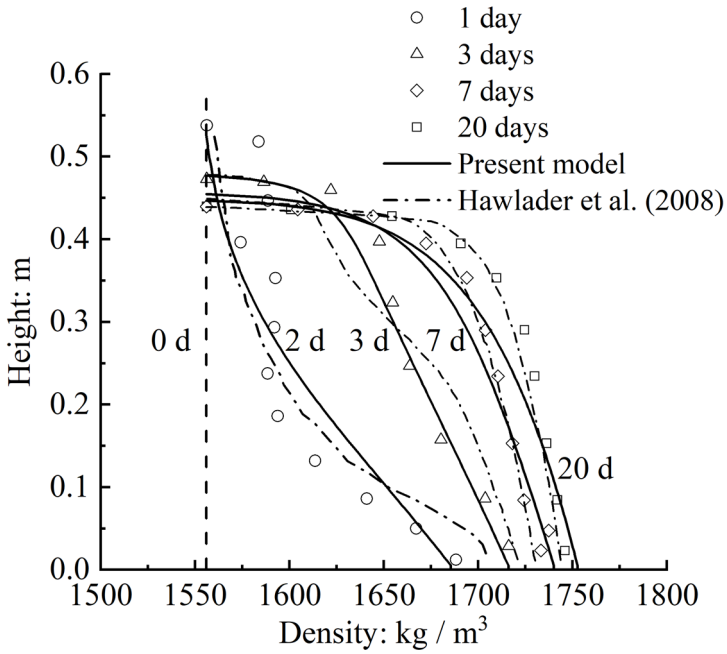

551

552 Figure 14–Predicted and measured density, Sidc 3 (Barhtolomeeusen et al., 2002; Hawlader et al., 2008)

553 The preceding numerical modelling case studies mainly reflect Class A prediction, which
554 might be not as convincing as Class C. Accordingly, Sidc 1 of Case Study 2 is also simulated
555 to verify the reliability of current 1D finite strain theory that takes into account creep for Class
556 C predictions. Figure 15 and Figure 16 show the settlement and predicted density distribution
557 of Sidc 1. The predicted results were compared with the test data of Sidc 1 and the best
558 numerical simulation results obtained by Znidarcic and Winterwerp at the Sidere held in
559 Oxford in 2000. The better agreement with test data than in Znidarcic and Winterwerp's results
560 further illustrates the reliability of present 1D finite strain theory for Class C prediction.

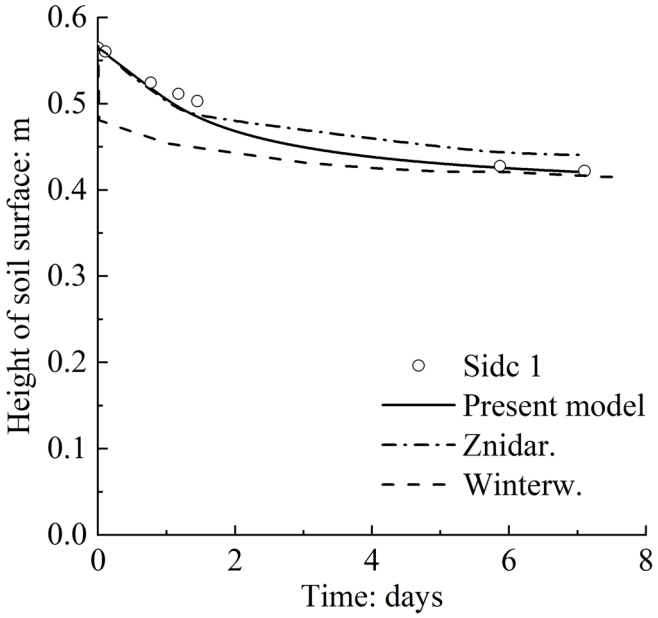

561

562 Figure 15–Predicted and measured settlement, Sidc 1 (Barhtolomeeusen et al., 2002)

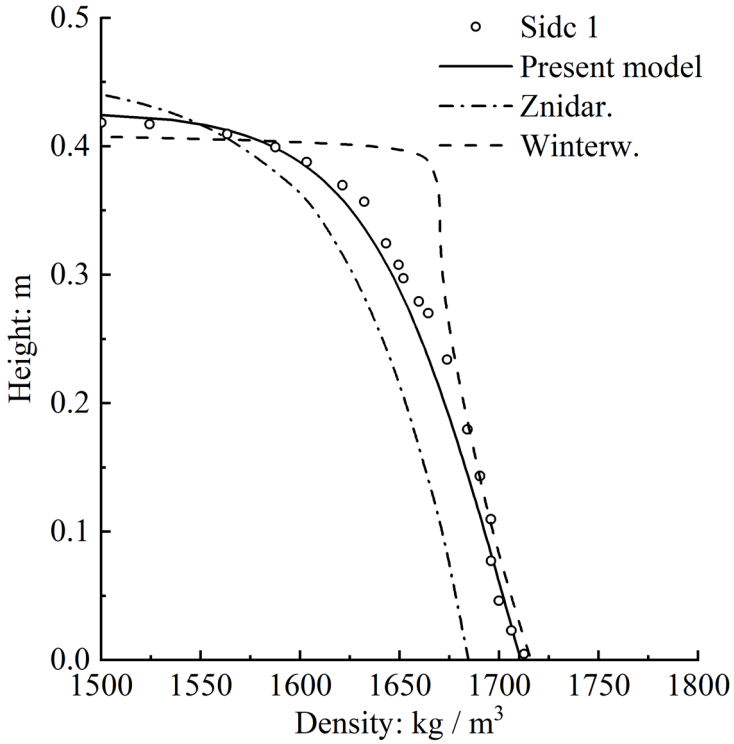

563

564 Figure 16–Predicted and measured density, Sidc 1 (Barhtolomeeusen et al., 2002)

565 **Case Study 3**

566 In this section, a 10 m standpipe test reported by Jeeravipoolvarn et al. (2009) was selected
567 as an application example to further demonstrate the applicability of the proposed model. The
568 tailings properties used in the standpipe test 1 were found from Jeeravipoolvarn et al. (2009).
569 The typical value t_0 = 1 day was simply taken. The ψ=0.041 was obtained by fitting. From the
570 standpipe test 1, the Figure (18) reported by Jeeravipoolvarn et al. (2009) was used to determine
571 the values of κ and λ as 0.142 and 1.030, respectively. The point $\left(\sigma'_p, e_p^{ep}\right)$ was determined as
572 (0.33 kPa,4.93). In addition, using Eq.(27) to draw a best–fit line through the permeability
573 profiles of the standpipe test 1, the relationship between the permeability coefficient and void
574 ratio was determined by k=4.32×10^{-7}(1+e)$^{4.93}$ m/day. All parameters were used to predict the
575 self-weight consolidation. Figure 17 and Figure 18 present the comparison between the
576 simulated and observed settlement and excess pore water pressure respectively. The total
577 consolidation time is about 10 years. Good agreement between measurements and predictions
578 for both settlement and excess pore water pressure was obtained.

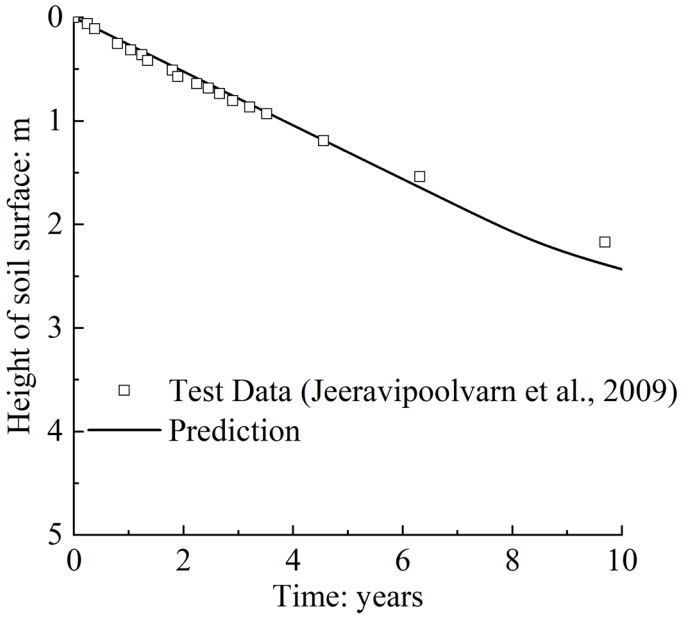

579

580 Figure 17–Comparison between measured and predicted settlement for standpipe 1 of Jeeravipoolvarn et

581 al. (2009)

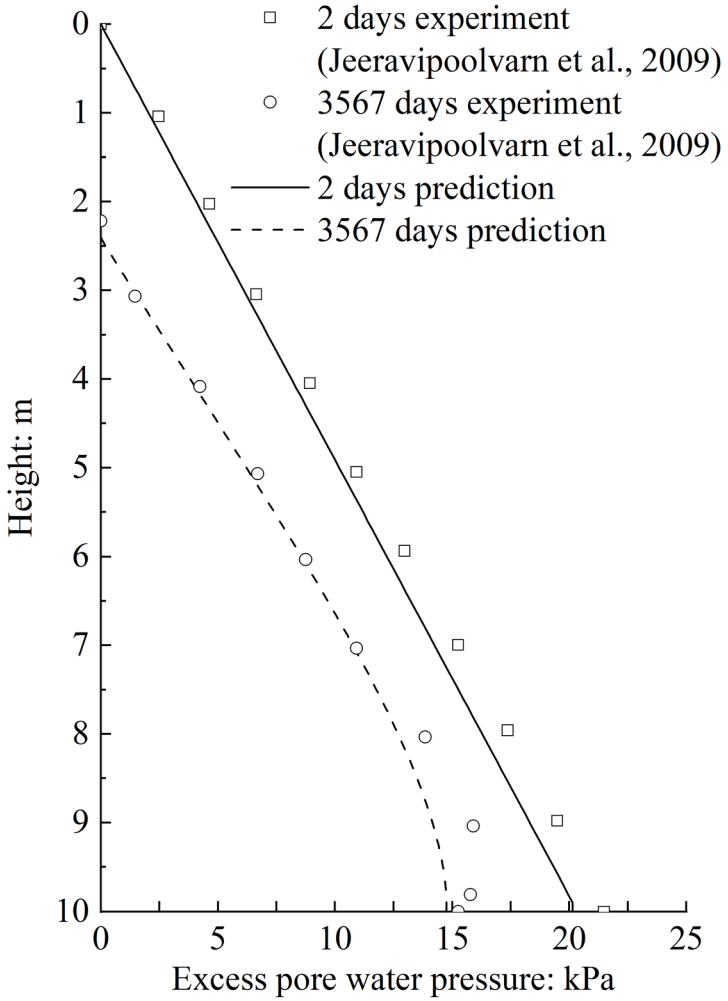

582

583 Figure 18–Comparison between measured and predicted excess pore water pressure for standpipe 1 of

584 Jeeravipoolvarn et al. (2009)

585 ## Parametric studies

586 The initial height and initial void ratio are generally recognized as state variables that

587 influence the self-weight consolidation of soil (Been and Sills, 1981; Bonin et al., 2014; Zhang

588 et al., 2022). They are also critical design parameters in an engineering project, and thus are

589 chosen for parametric study with other parameters kept constant. The values of κ, λ, and ψ are

590 0.2, 1, and 0.04, respectively. The typical value t_0 = 1 day was simply taken. The point $\left(\sigma'_p, e_p^{ep}\right)$

591 was taken as (0.2 kPa, 5). The permeability coefficient function was k=8.64×10^{-6}(1+e)^4 m/day.

592 Figures 19(a)-(c) show the influence of the soil's initial height (i.e. 1 m, 2 m and 3 m, all

593 with initial void ratio of 5) on the self-weight consolidation process. Interestingly, the soil

594 column with the smallest initial height has the smallest void ratio at the same relative depth on

595 the 100th day of self-weight consolidation. This is because the consolidation is faster when the

596 initial height is smaller, as shown in Figure 19(c). The average consolidation degrees of the

597 soil columns with three initial heights were 65.9%, 35.2%, and 20.6%, respectively. However,

598 As the consolidation continues, such as on the 1000th and 10000th day, the soil column with

599 higher initial height has smaller void ratio at the same relative depth. This is because, the soil

600 column with bigger initial height has bigger effective stress due to more soil quantity and higher

601 initial excess pore water pressure. Higher excess pore pressure dissipated would cause bigger

602 effective stress and result in smaller void ratio. The total settlements on the 10000th day of the

603 three cases are 0.333 m, 0.875 m, and 1.508 m respectively with the corresponding vertical

604 strains of 33.3%, 43.8% and 50.3% (Figure 19(b)). Overall, the effect of initial height on the

605 consolidation process is significant.

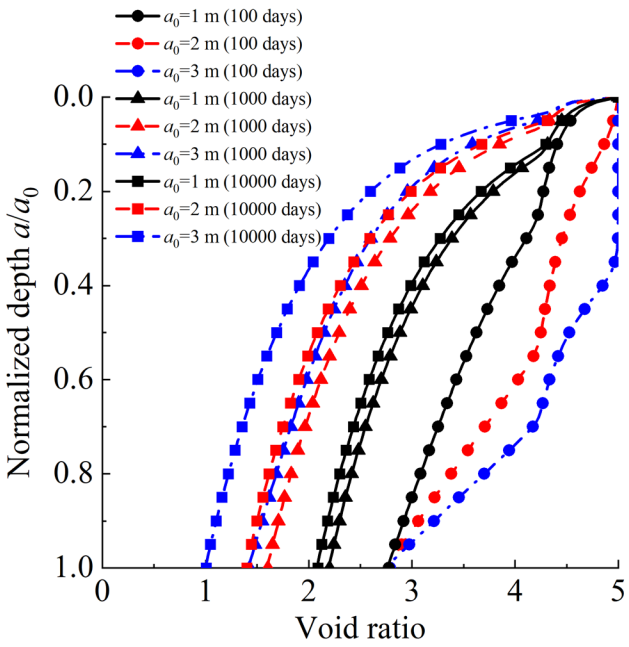

606

607 (a)

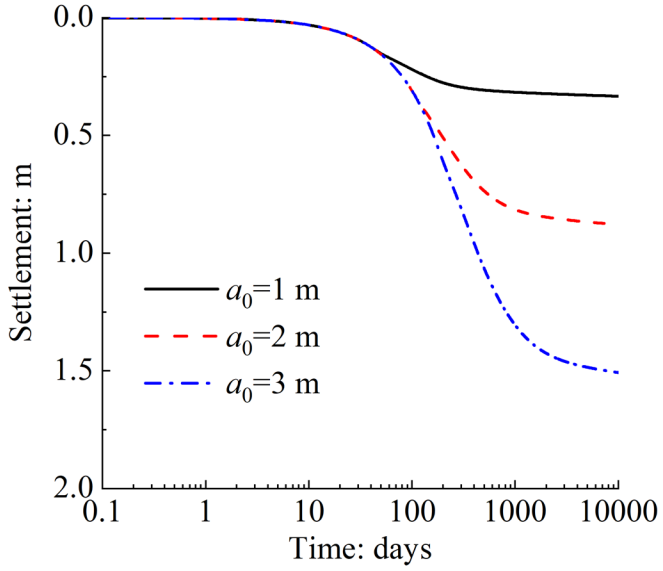

608

609 (b)

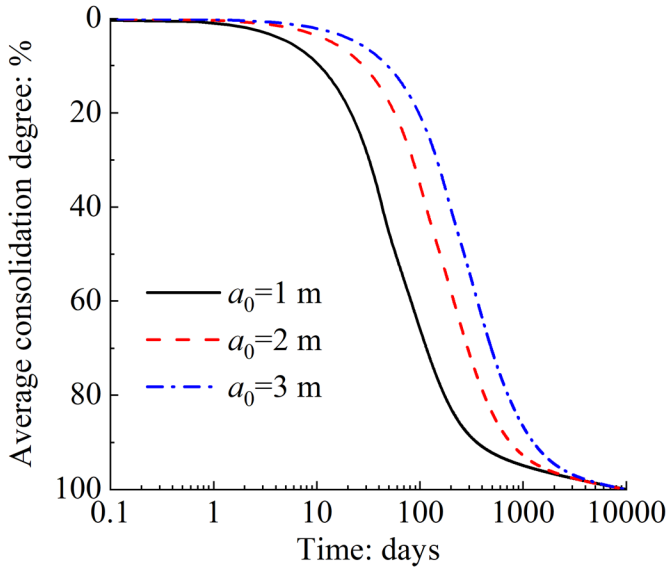

(c)

Figure 19– Consolidation process of slurry with different initial heights for evolutions of: (a) void ratio distribution; (b) settlement; and (c) average consolidation degree

Figures 20(a)-(c) show how the initial void ratio affects the self-weight consolidation process of slurry. In these simulations, the initial void ratios are 3, 4, and 5 with an identical initial height of 2 m. The total settlement of soil on the 10000th day is 0.673 m, 0.760 m, and 0.875 m respectively (Figure 20(b)). The time required to complete 90% of the consolidation is 1452 days, 1208 days, and 752 days respectively (Figure20(c)). In general, the soil column with bigger void ratio has bigger settlement but still bigger void ratio during consolidation. The effect of initial void ratio on the consolidation speed is significant. The consolidation speed of the soil column increases with the initial void ratio.

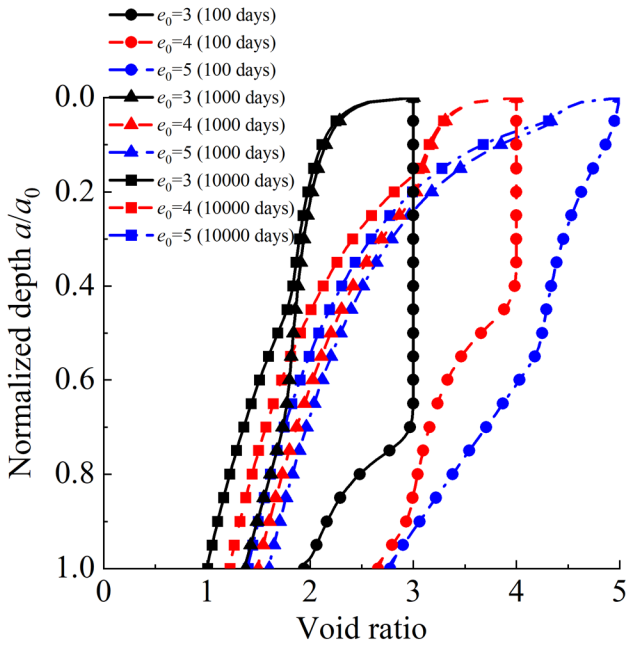

622

623 (a)

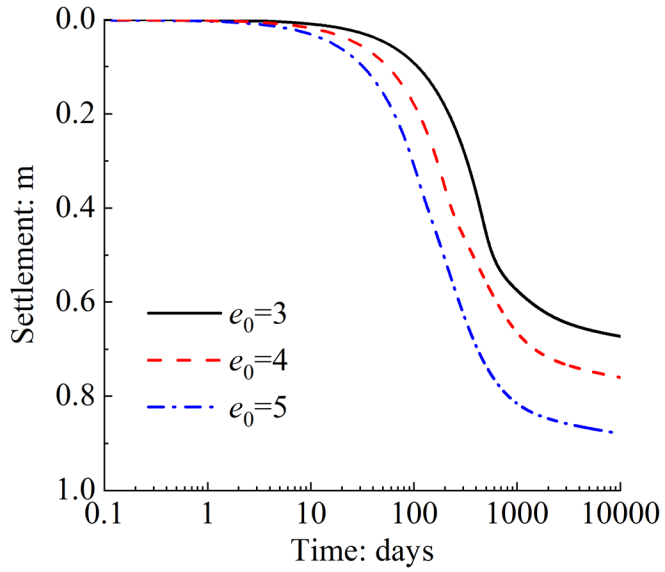

624

625 (b)

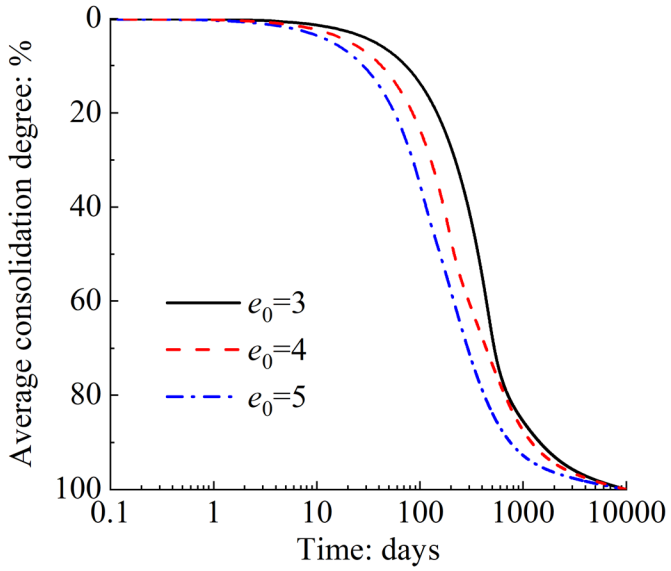

(c)

Figure 20– Consolidation process of slurry with different initial void ratios for evolution of: (a) void ratio distribution; (b) settlement; and (c) average consolidation degree

Conclusions

Yin-Graham one-dimensional Elastic Visco-Plastic (1D EVP) model has firstly been extended for finite strain modelling of self-weight consolidation of very soft clays. The extended EVP model inherits all the advantages of the original model, which can describe 1D stress or strain responses in soft soils exhibiting creep under general conditions including multistage loading, continuous loading, and unloading or reloading while overcoming the original model's limitation of being meaningless when the initial effective stress is very low or even zero.

Partial differential equations for 1D finite strain consolidation of very soft clays using the 1D EVP model have all been derived, in which nonlinear compressibility and permeability of

very soft soil skeleton are also taken into account. The Crank–Nicholson finite difference method has been used to solve nonlinear partial differential equations set. Finally, the present 1D finite strain consolidation model using the extended 1D EVP constitutive model has been validated through three case studies, which covers large initial void ratio of 5.17 and 9.87 and smaller initial void ratios of 2.094 and 2.475. The influences of some important parameters such as initial height and void ratio on the self-weight consolidation process are also analyzed. Comparing the prediction results with test data and numerical results of other researchers, the following conclusions can be drawn:

(a) There is a good agreement between predicted and measured results, confirming that the proposed 1D finite strain consolidation model can simulate changes in surface settlement, excess pore water pressure, total stress, void ratio and density distribution with time and space with good accuracy;

(b) The proposed model is reliable for finite strain consolidation analysis of very soft soils with a wide range of initial void ratios, and

(c) More importantly, the proposed model well captures the features of finite strain consolidation of very soft soils that the stress–strain relationships are not unique but rather are highly dependent on the locations or heights, surpassing which by taking into account the creep of these soft soils.

There are several deficiencies that need to be further studied. For example, in the proposed finite strain consolidation model, the influence of soil structure was not considered. Further

660 work can be conducted to extend the consolidation model for simulating the collapse of
661 structured soil by relating the creep characteristics to the structure change of clayey soil with
662 flocs. In addition, since there are few creep test data of clayey soil at very low-stress level
663 which is significant for expanding our understanding of the properties of soils, further
664 experimental studies should be conducted to investigate the creep behaviour of extremely soft
665 soil with high water content by improving the compressive testing apparatus. The proposed
666 finite strain consolidation model will be further extended to two- and three-dimensional to
667 assess the anisotropy of slurry treated using prefabricated vertical drains (PVD), prefabricated
668 horizontal drains (PHD), or other methods in practice.

669 **Acknowledgments:**

670 The work in this paper is supported by a Research Impact Fund (RIF) project (R5037-18), a
671 Theme-based Research Scheme Fund (TRS) project (T22-502/18-R), and three General
672 Research Fund (GRF) projects (PolyU 152179/18E; PolyU 152130/19E; PolyU 152100/20E)
673 from Research Grants Council (RGC) of Hong Kong Special Administrative Region
674 Government of China. The authors also acknowledge the financial supports from Research
675 Institute for Sustainable Urban Development of The Hong Kong Polytechnic University and a
676 grant ZDBS from The Hong Kong Polytechnic University.
677

678

679

680 **References**

681 Abu–Hejleh, A. N., Znidarčić, D., and Barnes, B. L. (1996). Consolidation characteristics of
682 phosphatic clays. Journal of Geotechnical Engineering, 122(4), 295–301. doi:
683 10.1061/(ASCE)0733–9410(1996)122:4(295).

684 Alexis, A., Bras, G. L., and Thomas, P. (2004). Experimental bench for study of settling–
685 consolidation soil formation. Geotechnical Testing Journal, 27(6), 557–567. doi:
686 10.1520/GTJ11582.

687 Bartholomeeusen, G., Sills, G. C., Znidarčić, D., Van Kesteren, W., Merckelbach, L. M., Pyke,
688 R., and Chan, D. (2002). Sidere: numerical prediction of large–strain
689 consolidation. Géotechnique, 52(9), 639–648. doi: 10.1680/geot.2002.52.9.639.

690 Been, K. (1980). Stress strain behaviour of a cohesive soil deposited under water [PhD thesis].

691 Been, K., and Sills, G. C. (1981). Self–weight consolidation of soft soils: an experimental and
692 theoretical study. Geotechnique, 31(4), 519–535. doi: 10.1680/geot.1981.31.4.519.

693 Berilgen, S. A., Berilgen, M. M., and Ozaydin, I. K. (2006). Compression and permeability
694 relationships in high water content clays. Applied Clay Science, 31(3–4), 249–261. doi:
695 10.1016/j.clay.2005.08.002.

696 Bjerrum, L. (1967). Engineering geology of Norwegian normally–consolidated marine clays
697 as related to settlements of buildings. Geotechnique, 17(2), 83–118. doi:
698 10.1680/geot.1967.17.2.83.

699 Bjerrum, L. (1973). Problems of soil mechanics and construction on soft clays and structurally
700 unstable soils. Proc International Conference on Soil Mechanics and Foundation
701 Engineering, 3, 111–159.

702 Bonin, M. D., Nuth, M., Dagenais, A. M., and Cabral, A. R. (2014). Experimental study and
703 numerical reproduction of self–weight consolidation behavior of thickened

704 tailings. Journal of Geotechnical and Geoenvironmental Engineering, 140(12), 04014068.
705 doi: 10.1061/(ASCE)GT.1943–5606.0001179.

706 Borja, R. I., and Alarcón, E. (1995). A mathematical framework for finite strain elastoplastic
707 consolidation Part 1: Balance laws, variational formulation, and linearization. Computer
708 Methods in Applied Mechanics and Engineering, 122(1–2), 145–171. doi: 10.1016/0045–
709 7825(94)00720–8.

710 Borja, R. I., Tamagnini, C., and Alarcon, E. (1994). Elasto–plastic consolidation at finite
711 strain. Computer methods and advances in geomechanics, 1, 753–758.

712 Borja, R. I., Tamagnini, C., and Alarcón, E. (1998). Elastoplastic consolidation at finite strain
713 part 2: finite element implementation and numerical examples. Computer Methods in
714 Applied Mechanics and Engineering, 159(1–2), 103–122. doi: 10.1016/S0045–
715 7825(98)80105–9.

716 Cargill, K. W. (1986). The large strain, controlled rate of strain (LSCRS) device for
717 consolidation testing of soft fine–grained soils. Technical Rep. GL–86–13, U.S. Army
718 Engineer Waterways Experiment Station Vicksburg, Miss.

719 Carrier III, W. D., Bromwell, L. G., and Somogyi, F. (1983). Design capacity of slurried
720 mineral waste ponds. Journal of Geotechnical Engineering, 109(5), 699–716. doi:
721 10.1061/(ASCE)0733–9410(1983)109:5(699).

722 Carter, J. P., Booker, J. R., and Small, J. C. (1979). The analysis of finite elasto–plastic
723 consolidation. International Journal for Numerical and Analytical Methods in
724 Geomechanics, 3(2), 107–129. doi: 10.1002/nag.1610030202.

725 Dolinar, B. (2009). Predicting the hydraulic conductivity of saturated clays using plasticity–
726 value correlations. Applied Clay Science, 45(1–2), 90–94. doi:
727 10.1016/j.clay.2009.04.001.

728 Feng, J., Ni, P., and Mei, G. (2019). One - dimensional self - weight consolidation with
729 continuous drainage boundary conditions: Solution and application to clay - drain

730 reclamation. International Journal for Numerical and Analytical Methods in
731 Geomechanics, 43(8), 1634-1652. doi: 10.1002/nag.2928.

732 Feng, J., Ni, P., Chen, Z., Mei, G., and Xu, M. (2020). Positioning design of horizontal drain
733 in sandwiched clay-drain systems for land reclamation. Computers and Geotechnics, 127,
734 103777. doi: 10.1016/j.compgeo.2020.103777.

735 Fox, P. J. (1996). Analysis of hydraulic gradient effects for laboratory hydraulic conductivity
736 testing. Geotechnical Testing Journal, 19(2), 181–190. doi: 10.1520/GTJ10340J.

737 Fox, P. J. (1999). Solution charts for finite strain consolidation of normally consolidated
738 clays. Journal of geotechnical and geoenvironmental engineering, 125(10), 847–867. doi:
739 10.1061/(ASCE)1090–0241(1999)125:10(847).

740 Fox, P. J., and Berles, J. D. (1997). CS2: a piecewise - linear model for large strain
741 consolidation. International Journal for Numerical and Analytical Methods in
742 Geomechanics, 21(7), 453–475. doi: 10.1002/(SICI)1096–9853(199707)21:7<453::AID–
743 NAG887>3.0.CO;2–B.

744 Fox, P. J., Pu, H. F., and Berles, J. D. (2014). CS3: Large strain consolidation model for layered
745 soils. Journal of Geotechnical and Geoenvironmental Engineering, 140(8), 04014041–
746 1~13. doi: 10.1061/(ASCE)GT.1943–5606.0001128.

747 Gibson, R. E., England, G. L., and Hussey, M. J. L. (1967). The theory of one–dimensional
748 consolidation of saturated clays: I. Finite non–linear consildation of thin homogeneous
749 layers. Geotechnique, 17(3), 261–273. doi: 10.1680/geot.1967.17.3.261.

750 Gibson, R. E., Schiffman, R. L., and Cargill, K. W. (1981). The theory of one–dimensional
751 consolidation of saturated clays. II. Finite nonlinear consolidation of thick homogeneous
752 layers. Canadian geotechnical journal, 18(2), 280–293. doi: 10.1139/t81–030.

753 Hawlader, B. C., Muhunthan, B., and Imai, G. (2003). Viscosity effects on one-dimensional
754 consolidation of clay. International Journal of Geomechanics, 3(1), 99-110. doi:
755 10.1061/(ASCE)1532-3641(2003)3:1(99).

Hawlader, B. C., Muhunthan, B., and Imai, G. (2008). State–dependent constitutive model and numerical solution of self–weight consolidation. Géotechnique, 58(2), 133–141. doi: 10.1680/geot.2008.58.2.133.

Hong, Z. S., Zeng, L. L., Cui, Y. J., Cai, Y. Q., and Lin, C. (2012). Compression behaviour of natural and reconstituted clays. Géotechnique, 62(4), 291-301. doi: 10.1680/geot.10.P.046.

Imai, G. (1981). Experimental studies on sedimentation mechanism and sediment formation of clay materials. Soils and foundations, 21(1), 7-20. doi: 10.3208/sandf1972.21.7.

Imai, G. (1995). Analytical examinations of the foundations to formulate consolidation phenomena with inherent time–dependence. In Compression and consolidation of clayey soils (pp. 891–935).

Indraratna, B., Baral, P., Rujikiatkamjorn, C., and Perera, D. (2018). Class A and C predictions for Ballina trial embankment with vertical drains using standard test data from industry and large diameter test specimens. Computers and Geotechnics, 93, 232–246. doi: 10.1016/j.compgeo.2017.06.013.

Indraratna, B., Baral, P., Rujikiatkamjorn, C., and Perera, D. (2018). Class A and C predictions for Ballina trial embankment with vertical drains using standard test data from industry and large diameter test specimens. Computers and Geotechnics, 93, 232-246.

Indraratna, B., Zhong, R., Fox, P. J., and Rujikiatkamjorn, C. (2017). Large-strain vacuum-assisted consolidation with non-Darcian radial flow incorporating varying permeability and compressibility. Journal of Geotechnical and Geoenvironmental Engineering, 143(1), 04016088. doi: 10.1061/(ASCE)GT.1943-5606.0001599.

Jeeravipoolvarn, S., Scott, J. D., and Chalaturnyk, R. J. (2009). 10 m standpipe tests on oil sands tailings: long-term experimental results and prediction. Canadian Geotechnical Journal, 46(8), 875-888. doi: 10.1139/T09-033.

780 Jin, Y. F., and Yin, Z. Y. (2020). An intelligent multi–objective EPR technique with multi–
781 step model selection for correlations of soil properties. Acta Geotechnica, 15(8), 2053–
782 2073. doi: 10.1007/s11440–020–00929–5.

783 Jin, Y. F., Yin, Z. Y., Zhou, W. H., Yin, J. H., and Shao, J. F. (2019). A single–objective EPR
784 based model for creep index of soft clays considering L2 regularization. Engineering
785 Geology, 248, 242–255. doi: 10.1016/j.enggeo.2018.12.006.

786 Kim, Y. T., and Leroueil, S. (2001). Modeling the viscoplastic behaviour of clays during
787 consolidation: application to Berthierville clay in both laboratory and field conditions.
788 Canadian Geotechnical Journal, 38(3), 484-497. doi: 10.1139/t00-108.

789 Kutilek, M. (1964). The filtration of water in soils in the region of the laminar flow. 8th Int.
790 Congr. ISSS, II, 45-52.

791 Kutilek, M. (1972). Non-darcian flow of water in soils—laminar region: a review.
792 Developments in Soil Science, 2, 327-340.

793 Kutter, B. L., and Sathialingam, N. (1992). Elastic-viscoplastic modelling of the rate-dependent
794 behaviour of clays. Géotechnique, 42(3), 427-441. doi: 10.1680/geot.1992.42.3.427.

795 Lambe, T. W. (1973). Predictions in soil engineering. Géotechnique, 23(2), 151–202. doi:
796 10.1680/geot.1973.23.2.151.

797 Leoni, M., Karstunen, M., and Vermeer, P. A. (2008). Anisotropic creep model for soft soils.
798 Géotechnique, 58(3), 215-226. doi: 10.1680/geot.2008.58.3.215.

799 Liu, Q., Deng, Y. B., and Wang, T. Y. (2018). One-dimensional nonlinear consolidation theory
800 for soft ground considering secondary consolidation and the thermal effect. Computers
801 and Geotechnics, 104, 22-28.

802 McNabb, A. (1960). A mathematical treatment of one–dimensional soil
803 consolidation. Quarterly of Applied Mathematics, 17(4), 337–347. doi:
804 10.1090/qam/113405.

McVay, M., Townsend, F., and Bloomquist, D. (1986). Quiescent consolidation of phosphatic waste clays. Journal of Geotechnical Engineering, 112(11), 1033–1049. doi: 10.1061/(ASCE)0733–9410(1986)112:11(1033).

Mei, G. X., Lok, T. M. H., Xia, J., and Wu, S. S. (2014). One-dimensional consolidation with asymmetrical exponential drainage boundary. Geomechanics and Engineering, 6(1), 47-63. doi: 10.12989/GAE.2014.6.1.047.

Mei, G., Feng, J., Xu, M., & Ni, P. (2022). Estimation of Interface Parameter for One-Dimensional Consolidation with Continuous Drainage Boundary Conditions. International Journal of Geomechanics, 22(3), 04021292. doi: 10.1061/(ASCE)GM.1943-5622.0002300.

Mesri, G., and Castro, A. (1987). C_α/C_c concept and K_0 during secondary compression. Journal of geotechnical engineering, 113(3), 230-247.

Miller, R. J., and Low, P. F. (1963). Threshold gradient for water flow in clay systems. Soil Science Society of America Journal, 27(6), 605-609.

Mitchell, J. K., and Soga, K. (2005). Fundamentals of soil behavior (Vol. 3, p. USA). New York: John Wiley & Sons.

Nash, D. (2001). Modelling the effects of surcharge to reduce long term settlement of reclamations over soft clays: a numerical case study. Soils and Foundations, 41(5), 1–13. doi: 10.3208/sandf.41.5_1.

Nash, D. F. T., and Ryde, S. J. (2001). Modelling consolidation accelerated by vertical drains in soils subject to creep. Géotechnique, 51(3), 257–273. doi: 10.1680/geot.2001.51.3.257.

Olsen, H. W. (1985). Osmosis: a cause of apparent deviations from Darcy's law. Canadian Geotechnical Journal, 22(2), 238-241.

Pane, V., and Schiffman, R. L. (1997). The permeability of clay suspensions. Geotechnique, 47(2), 273–288. doi: 10.1680/geot.1997.47.2.273.

Pu, H. F., Fox, P. J., Shackelford, C. D., and Qiu, J. (2021). Assessment of Consolidation–Induced Contaminant Transport for In Situ Capping of Subaqueous Contaminated Sediments. Journal of Geotechnical and Geoenvironmental Engineering, 147(8), 04021056. doi: 10.1061/(ASCE)GT.1943–5606.0002564.

Pu, H. F., Wang, K., Qiu, J., and Chen, X. (2020). Large-strain numerical solution for coupled self-weight consolidation and contaminant transport considering nonlinear compressibility and permeability. Applied Mathematical Modelling, 88, 916-932. doi: 10.1016/j.apm.2020.07.010

Pu, H., Song, D., and Fox, P. J. (2018). Benchmark problem for large strain self-weight consolidation. Journal of Geotechnical and Geoenvironmental Engineering, 144(5), 06018002.

Pu, H., Yang, P., Lu, M., Zhou, Y., and Chen, J. N. (2020). Piecewise-linear large-strain model for radial consolidation with non-Darcian flow and general constitutive relationships. Computers and Geotechnics, 118, 103327. doi: 10.1016/j.compgeo.2019.103327.

Richard, F. E. (1957). A review of the theories for sand drains. Journal of the Soil Mechanics and Foundations Division, 83(3), 1–38. doi: 10.1061/JSFEAQ.0000064.

Schiffman, R. L. (1980). Finite and infinitesimal strain consolidation. Journal of the Geotechnical Engineering Division, 106(2), 203–207. doi: 10.1061/AJGEB6.0000924.

Sills, G. (1998). Development of structure in sedimenting soils. Philosophical Transactions of the Royal Society of London. Series A: Mathematical, Physical and Engineering Sciences, 356(1747), 2515–2534. doi: 10.1098/rsta.1998.0284

Sills, G. C. (1995). Time dependent processes in soil consolidation. In Compression and consolidation of clayey soils (pp. 875–890).

Stark, T. D., Choi, H., and Schroeder, P. R. (2005). Settlement of dredged and contaminated material placement areas. II: Primary consolidation, secondary compression, and

855 desiccation of dredged fill input parameters. Journal of Waterway, port, coastal, and ocean
856 engineering, 131(2), 52–61. doi: 10.1061/(ASCE)0733–950X(2005)131:2(52).

857 Stolle, D. F. E., Vermeer, P. A., and Bonnier, P. G. (1999). A consolidation model for a
858 creeping clay. Canadian geotechnical journal, 36(4), 754-759. doi: 10.1139/t99-034.

859 Terzaghi, K. (1943). Theoretical Soil Mechanics. New York: Wiley.

860 Vermeer, P.A., and Neher, H.P., 1999. A soft soil model that accounts for creep. In:
861 Proceedings of the Plaxis Symposium on Beyond 2000 in Computational Geotechnics,
862 Amsterdam, pp. 249–262.

863 Vrakas, A., and Anagnostou, G. (2015). A simple equation for obtaining finite strain solutions
864 from small strain analyses of tunnels with very large convergences. Géotechnique, 65(11),
865 936-944. doi: 10.1680/jgeot.15.P.036.

866 Wang, J., Ding, J., Wang, H., and Mou, C. (2020). Large-strain consolidation model
867 considering radial transfer attenuation of vacuum pressure. Computers and Geotechnics,
868 122, 103498.

869 Winterwerp, J. C. (1999). On the dynamics of high-concentrated mud suspensions. PhD thesis,
870 Delft University of Technology.

871 Xu, G., Gao, Y., Yin, J., Yang, R., and Ni, J. (2015). Compression behavior of dredged slurries
872 at high water contents. Marine Georesources & Geotechnology, 33(2), 99-108. doi:
873 10.1080/1064119X.2013.805287.

874 Yin, J. H. (1999). Properties and behaviour of Hong Kong marine deposits with different clay
875 contents. Canadian Geotechnical Journal, 36(6), 1085–1095. doi: 10.1139/t99–068.

876 Yin, J. H. (1999). Properties and behaviour of Hong Kong marine deposits with different clay
877 contents. Canadian Geotechnical Journal, 36(6), 1085-1095.

878 Yin, J. H. (2015). Fundamental issues of elastic viscoplastic modeling of the time–dependent
879 stress–strain behavior of geomaterials. International Journal of Geomechanics, 15(5),
880 A4015002. doi: 10.1061/(ASCE)GM.1943–5622.0000485.

881 Yin, J. H., and Graham, J. (1989). Visco–elastic–plastic modelling of one–dimensional time–
882 dependent behaviour of clays. Canadian Geotechnical Journal, 26(3), 199–209. doi:
883 10.1139/t89–029.

884 Yin, J. H., and Graham, J. (1994). Equivalent times and one–dimensional elastic viscoplastic
885 modelling of time–dependent stress–strain behaviour of clays. Canadian Geotechnical
886 Journal, 31(1), 42–52. doi: 10.1139/t94–005.

887 Yin, J. H., and Graham, J. (1996). Elastic visco–plastic modelling of one–dimensional
888 consolidation. Geotechnique, 46(3), 515–527. doi: 10.1680/geot.1996.46.3.515.

889 Yin, J. H., and Zhu, G. F. (2020). Consolidation Analyses of Soils (1st ed.). London: CRC
890 Press.

891 Yin, Z. Y., and Wang, J. H. (2012). A one-dimensional strain-rate based model for soft
892 structured clays. Science China Technological Sciences, 55(1), 90-100. doi:
893 10.1007/s11431-011-4513-y.

894 Yin, Z. Y., Chang, C. S., Karstunen, M., and Hicher, P. Y. (2010). An anisotropic elastic–
895 viscoplastic model for soft clays. International Journal of Solids and Structures, 47(5),
896 665-677. doi: 10.1016/j.ijsolstr.2009.11.004.

897 Yin, Z. Y., Jin, Y. F., Huang, H. W., and hen, S. L. (2016). Evolutionary polynomial regression
898 based modelling of clay compressibility using an enhanced hybrid real–coded genetic
899 algorithm. Engineering Geology, 210, 158–167. doi: 10.1016/j.enggeo.2016.06.016.

900 Zeng, L. L., Cai, Y. Q., Cui, Y. J., and Hong, Z. S. (2020). Hydraulic conductivity of
901 reconstituted clays based on intrinsic compression. Géotechnique, 70(3), 268–275. doi:
902 10.1680/jgeot.18.P.096.

Zhang, P., Yin, Z. Y., Jin, Y. F., and Chan, T. H. (2020). A novel hybrid surrogate intelligent model for creep index prediction based on particle swarm optimization and random forest. Engineering Geology, 265, 105328.

Zhang, H., Liu, S., Sun, H., Cai, Y., Geng, X., Pan, X., and Deng, Y. (2022). Large-Strain Self-Weight Consolidation of Dredged Sludge. International Journal of Geomechanics, 22(1).

Zhu, G. F., and Yin, J. H. (1999). Finite element analysis of consolidation of layered clay soils using an elastic visco-plastic model. International Journal for Numerical and Analytical Methods in Geomechanics, 23(4), 355–374. doi: 10.1002/(SICI)1096–9853(19990410)23:4<355::AID–NAG975>3.0.CO;2–D.

Znidarcic, D., Croce, P., Pane, V., Ko, H. Y., Olsen, H. W., and Schiffman, R. L. (1984). The theory of one–dimensional consolidation of saturated clays: III. existing testing procedures and analyses. Geotechnical Testing Journal, 7(3), 123–134. doi : 10.1520/GTJ10488J.

Znidarčić, D., Schiffman, R. L., Pane, V., Croce, P., Ko, H. Y., and Olsen, H. W. (1986). The theory of one–dimensional consolidation of saturated clays: part V, constant rate of deformation testing and analysis. Géotechnique, 36(2), 227–237. doi: 10.1680/geot.1986.36.2.227.